NASA MEMO 10-23-58L

NASA

MEMORANDUM

EFFECTS OF BODY SHAPE ON THE DRAG OF A 45° SWEPTBACK-WING—BODY CONFIGURATION AT MACH NUMBERS FROM 0.90 TO 1.43

By Walter B. Olstad and Thomas L. Fischetti

Langley Research Center
Langley Field, Va.

NATIONAL AERONAUTICS AND SPACE ADMINISTRATION
WASHINGTON
November 1958
Declassified April 12, 1961

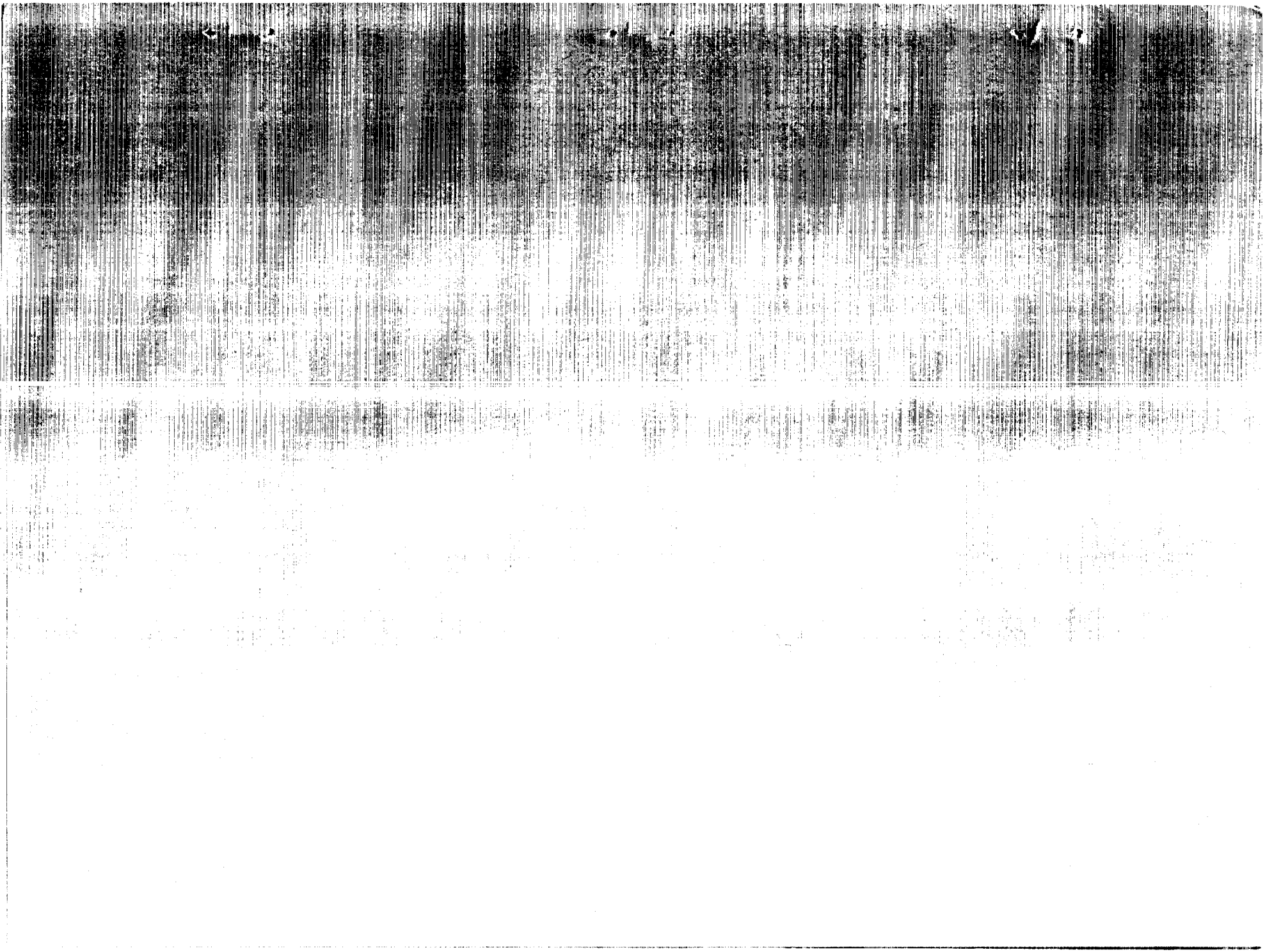

NATIONAL AERONAUTICS AND SPACE ADMINISTRATION

NASA MEMO 10-23-58L

EFFECTS OF BODY SHAPE ON THE DRAG OF A 45° SWEPTBACK-WING—BODY CONFIGURATION AT MACH NUMBERS FROM 0.90 TO 1.43*

By Walter B. Olstad and Thomas L. Fischetti

SUMMARY

An investigation was made of the effects of body shape on the drag of a 45° sweptback-wing—body combination at Mach numbers from 0.90 to 1.43.

Both the expansion and compression fields induced by body indentation were swept back as the stream Mach number increased from 0.94. The line of zero pressure change was generally tangent to the Mach lines associated with the local velocities over the wing and body. The strength of the induced pressure fields over the wing were attenuated with spanwise distance and the major effects were limited to the inboard 60 percent of the wing semispan.

Asymmetrical body indentation tended to increase the lift on the forward portion of the wing and reduce the lift on the rearward portion. This redistribution of lift had a favorable effect on the wave drag due to lift. Symmetrical body indentation reduced the drag loading near the wing-body juncture at all Mach numbers. The reduction in drag loading increased in spanwise extent as the Mach number increased and the line of zero induced pressure became more nearly alined with the line of maximum wing thickness.

Calculations of the wave drag due to thickness, the wave drag due to lift, and the vortex drag of the basic and symmetrical $M = 1.2$ body and wing combinations at an angle of attack of 0° predicted the effects of indentation within 11 percent of the wing—basic-body drag throughout the Mach number range from 1.0 to 1.43. Calculations of the wave drag due to thickness, the wave drag due to lift, and the vortex drag for the basic, symmetrical $M = 1.2$, and asymmetrical $M = 1.4$ body and wing combinations predicted the total pressure drag to within 8 percent

*Title, Unclassified.

of the experimental value at $M = 1.43$. The incremental pressure drag due to a symmetrical $M = 1.2$ indentation was predicted to within 8 percent of the total pressure drag of the wing-indented body combination for all Mach numbers above $M = 1.0$.

A theoretical method presented herein proved useful in predicting the distributions of the oblique section lift parameter, $\beta l/2q$. The differences in wave drag due to lift calculated from the predicted and experimental distributions of $\beta l/2q$, were less than 6 percent of the total pressure drag.

INTRODUCTION

The transonic area rule (ref. 1) provides a means for reducing the zero-lift wave drag of wing-body combinations at Mach numbers near 1. An extension of the area-rule concept led to a supersonic area rule (refs. 2 and 3) that has proven useful in reducing the zero-lift wave drag at higher speeds. The zero-lift wave drag of a wing-body combination is related, by the supersonic area rule, to the wave drags of a series of equivalent bodies. The equivalent-body shapes are determined by the area distribution of the wing-body combination. The area rule, as presented in references 2 and 3, neglects the reflection of disturbances by the wing, but for unsymmetrical configurations, this introduces errors. Reference 4 suggests including these effects by considering separately the area distributions above and below the wing-chord plane. Application of this concept decreased the drag significantly for two unsymmetrical configurations.

Reference 5 considers the wave drag of a lifting wing-body combination at supersonic speeds. The wave drag is again related to the wave drags of a series of equivalent bodies of revolution, but in this case, the equivalent-body shapes depend on both the pressure distribution and the area distribution of the wing-body combination.

In the past, experimental studies of the area rule have been confined largely to measurements of overall forces. The present paper discusses the effects of body shaping on the distribution of drag. A 45° sweptback wing has been tested in combination with four different bodies at a Mach number of 1.43 and with two of these bodies at Mach numbers from 0.8 to 1.43. The pressure distributions are studied to determine the magnitude and extent of the pressure field due to both symmetrical and asymmetrical body indentations and to determine the locations on the wing and body where the drag is reduced as a result of the indentations. In addition, experimental drag values for asymmetrical and lifting configurations are compared for the first time with values calculated by

methods based on references 4 and 5 and by a modified method presented herein.

SYMBOLS

b	wing span, 28.478 in.
c	local chord, in.
$\bar{c}$	mean aerodynamic chord, 8.42 in.
c_{av}	average wing chord, 7.12 in.
c_d	section drag coefficient
C_D	total drag coefficient, $\frac{\text{Drag}}{qSw}$
$C_{D,f}$	skin-friction drag coefficient
$C_{D,p}$	integrated pressure drag coefficient
C_{D,w_o}	wave drag coefficient due to thickness
$C_{D,w}$	wave drag coefficient due to lift
$C_{D,w,\theta}$	incremental wave drag coefficient due to lift
$C_{D,v}$	vortex drag coefficient
C_L	lift coefficient, $\frac{\text{Lift}}{qSw}$
c_n	section normal-force coefficient
C_p	local pressure coefficient
ΔC_p	differential pressure coefficient
c_x	section chord-force coefficient
h	vertical dimension, in. (see fig. 8)

l or $l(x,\theta)$ oblique section lift

M free-stream Mach number

q free-stream dynamic pressure

R body radius

R_{max} maximum body radius

$\Delta R'$ change in body slope, dR/dx

S or $S(x,\theta)$ cross-sectional area, sq in.

S_w wing-plan-form area, 1.408 sq ft

U free-stream velocity

x,y,z Cartesian coordinate system

x_o axial distance from wing apex to intersection of Mach cutting plane with x-axis

α angle of attack, deg

α_s wing-section angle of attack, deg

$\beta = \sqrt{M^2 - 1}$

Γ total circulation developed by a given chordwise section of wing

θ cutting-plane roll angle, deg

Λ angle between the wing leading edge and the y-axis, deg

ξ auxiliary coordinate in x-direction, in.

ψ angle between intersection of Mach cutting plane with horizontal plane and x-axis

$\beta l/2q$ oblique-section lift parameter, in.

Subscripts:

a due to asymmetry about wing-chord plane

B	body
t	due to thickness
W	wing
WB	wing-body combination
α	due to angle of attack

Primes indicate differentiation with respect to x.

MODEL CONFIGURATIONS

The wing used in this investigation had an aspect ratio of 4.0 and a taper ratio of 0.15. The wing section varied linearly in thickness from a NACA 65A206, $a = 0$ section at the root to a NACA 65A203, $a = 0.8$ (modified) section at 50 percent of the semispan. Then the wing section remained constant to the tip. The wing was tested in conjunction with four body shapes. A sketch of the wing with a basic Sears-Haack body and a body indented symmetrically for a Mach number of 1.2 is shown in figure 1. The other two bodies, one with a symmetrical $M = 1.4$ indentation and one with an asymmetrical $M = 1.4$ indentation, are shown together with the wing in figure 2. The symmetrical $M = 1.4$ body has a cylindrical shape in the region of the wing-body juncture. Consideration of the effects of angle of attack led to the design of the asymmetrical body, which is indented on the upper surface but which actually has a bulge on the lower surface. Ordinates for all the bodies are presented in table I.

For the remainder of this report, the four bodies will be designated as follows: The basic Sears-Haack body will be called the basic body; the body indented symmetrically for a Mach number of 1.2 will be called the symmetrical $M = 1.2$ body; the body indented symmetrically for a Mach number of 1.4 will be called the symmetrical $M = 1.4$ body; and the body indented asymmetrically for a Mach number of 1.4 will be called the asymmetrical $M = 1.4$ body.

For the transition-fixed tests, 0.10-inch transition strips were located at 10 percent of the chord on both upper and lower surfaces of the wing and at 10 percent of body length. The strips were obtained by spraying the surfaces with a commercial liquid plastic and blowing on carborundum grains (approximately 0.012 inch in diameter) at an estimated density of 40 grains per inch.

DATA AVAILABLE FOR ANALYSIS

Force data have been published in reference 6 for the basic and $M = 1.2$ symmetrically indented configurations with both fixed and natural transition at Mach numbers from 0.80 to 1.43. Pressure distributions have been published in reference 7 for these same two configurations with transition fixed.

Additional pressure distributions for the basic and $M = 1.2$ symmetrical indentations with transition natural, and for the symmetrical and asymmetrical $M = 1.4$ indentations with transition fixed, were obtained in recent tests at a Mach number of 1.43. These tests were made in the Langley 8-foot transonic pressure tunnel where the supersonic Mach number of 1.43 is obtained by enclosing the longitudinal slots with specially designed channels that convert the slotted test section to a supersonic nozzle. Details of the resulting nozzle shape and of the test-section Mach number distributions have been published in reference 8. For these tests, the angles of attack were -2°, 0°, 2°, and 4°. Pressure distributions were obtained at six wing stations, 12, 25, 40, 60, 80, and 95 percent of the wing semispan, and at five longitudinal rows of body orifices, which were spaced at intervals of 45° and designated as rows A, B, C, D, and E. The rows of body orifices were lettered starting with row A on the center line along the upper surface and progressing in a clockwise direction while facing downstream. The orifice locations are given in reference 7. The results of these tests are presented herein in the form of pressure coefficients in figures 3 and 4.

METHOD OF ANALYSIS

The purpose of this section is to describe the methods by which the wave drag due to thickness, the wave drag due to lift, the vortex drag, the integrated pressure drag, and the skin-friction drag were either calculated or derived.

Wave drag.- Area distributions for the combinations with the basic body and the symmetrical $M = 1.2$ body have been presented in reference 6 for Mach numbers of 1.0, 1.2, and 1.4. These area distributions obtained in the normal manner (ref. 2) are identical for cuts taken at angles θ and $180^\circ - \theta$. Furthermore, they are the same area distributions that would be obtained if the wing were symmetrical (uncambered). The wave drag due to thickness has been calculated from these area distributions by means of the method of reference 9

Calculation of the wave drag for a lifting wing-body combination is more complex than for a nonlifting combination. In reference 5, the

wave drag is shown to be a function of $S''(x) - (\beta l'/2q)$, where $S''(x)$ is the second derivative of the cross-sectional area distribution and $\beta l'/2q$ is a function of the pressure distribution.

The calculation of the wave drag then requires the determination of both the cross-sectional area distribution and the distribution along the streamwise axis of the quantity l. For the $\theta = \theta_1$ cut, this quantity l is the component, normal to the free stream and parallel to the plane $\theta = \theta_1$, of the net resultant force on a section formed by the intersection of a Mach plane for the θ_1 cut with the configuration surface (ref. 5).

In the present analysis, several simplifying assumptions have been made in determining the distributions of $\beta l/2q$. These may be listed as follows:

(1) The wind axes specified in the theory were replaced by body axes in the calculations for an angle of attack of 4°.

(2) The side force determined by the integration of the pressures in the y-direction was neglected in obtaining the net resultant force. (For one case that was checked, calculations of the magnitude of this side force for $\theta = 90^\circ$, at which point it would be a maximum, indicated that the net effect on the drag was negligible.)

(3) In determining the streamwise distribution of $\beta l/2q$, only the region between the wing apex and the intersection of the cutting plane from the wing-tip trailing edge with the body center line was considered. (Calculations for $\alpha = 4^\circ$ using a distribution of this type and also a distribution that started at the body nose showed that omitting the lift on the forebody had only a small effect on the wave drag.)

Utilizing the second of these assumptions and the fact that the wing-body combination is symmetrical about the x,z-plane, the quantity l' can be shown to have the following property:

$$l'\left(x,\frac{\pi}{2} - \theta\right) = -l'\left(x,\theta - \frac{\pi}{2}\right)$$

that is, $l'(x,\theta)$ is an odd function of $\frac{\pi}{2} - \theta$. Also, because of symmetry, the term $S''(x,\theta)$ is seen to be an even function of $\frac{\pi}{2} - \theta$. If the terms $S''(x,\theta)$ and $l'(x,\theta)$ have the abovementioned properties, reference 5 shows that the wave drag due to thickness and the wave drag due to lift can be analyzed separately. All the wing-body combinations discussed in this paper will be analyzed in this manner. The error

in calculating the wave drag due to lift (introduced by the above mentioned assumptions) has been determined and was found to be less than 2 percent.

The $\beta l/2q$ distributions, as determined from pressure distributions at an angle of attack of 4°, are shown in figure 5 for the wing-basic body combination at several Mach numbers and values of θ. Distributions of $\beta l/2q$ for the asymmetrical $M = 1.4$ body and wing combination at a Mach number of 1.43 and for the symmetrical $M = 1.2$ body and wing combination at Mach numbers of 1.43 and 1.125 are compared in figure 6 with the distributions for the basic body. The incremental wave drag due to lift was calculated for each distribution by the method that is given in reference 9 for calculating the wave drag due to thickness from distributions of $S'(x)$. The distribution of the incremental wave drag due to lift with θ was then integrated to obtain the total wave drag due to lift.

Recently, it has been suggested (ref. 4) that for asymmetrical wing locations and for cambered wings the wing should be considered as a reflection plane and the areas above and below the wing-chord plane should be treated separately. This procedure is based on the consideration of a wing with an attached leading-edge shock wave, so that there is no communication between the upper and lower surface flow fields.

Let the area slope distribution for the $\theta = \theta_1$ cut, by the method of reference 4, be given by

$$S'(x,\theta_1)_t + S'(x,\theta_1)_a$$

where $S'(x,\theta_1)_t$ is derived from the area distribution of the complete model in the normal manner (ref. 2). The term $S'(x,\theta_1)_a$ is the contribution of the configuration asymmetry about the wing-chord plane and is derived from twice the difference in the area above and below the wing-chord plane.

Area distributions due to configuration asymmetry for a Mach number of 1.4 for the four wing-body combinations are presented in figure 7. The wave drag due to the configuration asymmetry has been calculated on the basis of these area distributions and the results will be presented in this paper.

It is now suggested that the method of reference 4 might be extended to the case of a wing-body combination at an angle of attack and that an equivalent area distribution due to angle of attack be found. This procedure will also be based on the consideration of a wing with an attached

leading-edge shock wave, so that there is no communication between the upper and lower surface flow fields.

The wing is assumed to be a flat plate (in the wing-chord plane) with an angle-of-attack distribution over the semispan. This distribution of angle of attack may be any combination of angle of attack of the body, wing incidence, wing twist, and effective twist due to body induced upwash. The cross-sectional area due to angle of attack for any value of x on the body axis is twice the projection normal to the free stream of the area on the cutting plane between the wing-chord plane and a plane parallel to the free-stream direction passing through the wing leading edge (see fig. 8). This area may be expressed mathematically as the integral of the height h on the projection over that portion of the semispan in which the cutting plane intersects the wing-chord plane or

$$S(x)_\alpha = 2\int_{y_1}^{y_2} h\, dy$$

From figure 8, it can be shown that $h = -\xi \tan \alpha$, and for small values of α, $h = -\xi\alpha$. Now

$$\xi = (\cot \psi - \tan \Lambda)y + x$$

Thus,

$$S(x)_\alpha = -2\int_{y_1}^{y_2} \left[(\cot \psi - \tan \Lambda)y + x\right]\alpha\, dy$$

Differentiating with respect to x yields

$$S'(x)_\alpha = -2\int_{y_1}^{y_2} \alpha\, dy$$

Therefore, the slope of the cross-sectional area distribution due to angle of attack of the wing is equal to twice the area under the curve of spanwise distribution of angle of attack between the limits y_1 and y_2. These limits are the points of interception of the Mach cutting plane with the boundaries of the exposed wing-chord plane, the inboard point being the lower limit.

The wave drag due to angle of attack has been calculated from the area slope of several of the wing-body combinations used in this investigation and the results have been presented in this paper.

Vortex drag.- The wave drag is derived in reference 5 by considering the transfer of momentum across a cylindrical surface of large radius that surrounds the lifting wing-body combination and extends far enough to the rear so that all the wave drag appears on the cylinder. The remaining drag can be found by considering the transfer of momentum across the end of this cylinder, a disk at a large distance downstream. At subsonic speeds, this part of the drag is normally referred to as induced drag, but this terminology seems inappropriate at supersonic speeds. The term vortex drag will be used throughout the entire speed range in this paper.

If the spanwise distribution of circulation Γ is known, the vortex drag can be evaluated by the following equation:

$$C_{D,v} = -\frac{1}{2\pi U^2 S_w} \int_{-b/2}^{b/2} \int_{-b/2}^{b/2} \Gamma'(y)\Gamma'(y_1)\log_e|y - y_1|\, dy\, dy_1$$

This equation has the same form as the wave-drag equation (ref. 5) and, consequently, the methods of reference 9 were used in its solution.

The spanwise distribution of circulation was found from the relation

$$\Gamma = \frac{c_{av}U}{2} c_n \frac{c}{c_{av}}$$

where $c_n \frac{c}{c_{av}}$ was determined from the pressure distribution over the surface of the wing-body combination (ref. 7).

Integrated pressure drag.- The integrated pressure drag coefficients were calculated from the pressure distributions by use of the following equations:

$$(C_{D,p})_W = \int_{\frac{R_{mean}}{b/2}}^{1} \int_0^1 c_d \frac{c}{c_{av}} d\left(\frac{z}{c}\right) d\left(\frac{y}{b/2}\right)$$

$$(C_{D,p})_B = \frac{2\pi R_{max}^2}{S_w} \int_0^1 \int_0^1 C_p \frac{R}{R_{max}} d\left(\frac{\theta}{\pi}\right) d\left(\frac{R}{R_{max}}\right)$$

where $c_d = c_x \cos \alpha_s + c_n \sin \alpha_s$. The wing twisted appreciably under load because of aeroelastic effects (ref. 7). The section angle-of-attack distribution was calculated for each Mach number and angle of attack for the wing—basic-body combination using the section force

coefficients and wing-twist influence coefficients tabulated in reference 7. The section drag coefficients were then obtained by adding the components, in the drag direction, of the section chord-force and normal-force coefficients.

Skin-friction drag.- The skin-friction drag throughout the Mach number range was obtained by subtracting $(C_{D,p})_{WB}$ from the overall C_D obtained in the force tests of reference 6.

RESULTS AND DISCUSSION

Pressures Induced by Body Indentation

The difference between the pressure on a wing—basic-body combination and the pressure on a wing—indented-body combination can be considered as a pressure induced by changing the body shape. Contours of constant induced pressure coefficients ΔC_p are shown in figure 9 for the $M = 1.2$ indented-body combination at 0° angle of attack and several Mach numbers. The contours were obtained from pressure data in reference 7.

Pressures induced on body.- The differential body pressures in figure 9 show, as would be expected, an expansion over the forward part of the indentation, followed by a compression. The strength of the expansion on the body increases with increase in Mach number, becoming a maximum at $M = 1.03$, and then decreases with further increases in Mach number. The compression, however, is strongest at subsonic speeds and decreases with increase in Mach number. In both cases, the strength of the induced pressure field appears to be a maximum when the local Mach number in the vicinity of the body is approximately 1.0.

In reference 11, the induced pressure field is calculated by linearized theory for indented and bumped bodies for which the source distribution is given. When the body shape, rather than the source distribution, is given, the calculation of the pressure field is more difficult. In the limiting case on the surface of the body, however, the change in pressure coefficient can be obtained from the two-dimensional relation (ref. 11)

$$\Delta C_p = \frac{2}{\beta} \Delta R'$$

where $\Delta R'$ is the change in body slope. However, the pressure change calculated by this two-dimensional relation is displaced downstream. The pressures induced over the upper surface of the body by the symmetrical $M = 1.2$ indentation are compared in figure 10 with induced

pressures given by the two-dimensional relation for Mach numbers of 1.125 and 1.43. The calculated pressure distributions are not only displaced downstream, as expected, but the pressure coefficients also are of greater magnitude than the experimental values. Both theory and experiment show a decrease in induced pressure coefficient with Mach number.

Pressures induced on wing.- The location of the induced pressure field relative to the wing plan form varies greatly with free-stream Mach number (fig. 9). At a Mach number of 0.94, the induced pressure field extends more or less laterally across the wing. With increase in Mach number from 0.94, the expansion field from the forward portion of the indentation increases in spanwise extent and is swept back along the wing until, at a Mach number of 1.43, it covers the major portion of the wing. Likewise, the compression field, which is well forward on the wing at a Mach number of 0.94, is gradually swept back with increase in Mach number until it affects only a small portion of the inboard trailing-edge region of the wing at a Mach number of 1.43. The strength of the pressure fields over the wing is attenuated with spanwise distance. At a Mach number of 1.125, which is nearest the indentation design Mach number of 1.2, the induced pressure fields are felt at the wing tips, but, due to the attentuation, the major effects are limited to the inboard 60 percent of the semispan.

Line of zero pressure change.- The line of zero pressure change $\Delta C_p = 0$ is of particular interest because it represents the boundary between the expansion and compression fields. Examination of the actual pressure coefficients on the wing—indented-body combination indicates that this line is generally swept back so that it is tangent to the Mach lines associated with the local velocities over the wing and body. Obviously, the body indentation will be most effective in reducing the wing drag if this line is swept so as to coincide with the line of maximum wing thickness. At a Mach number of 1.125, the $\Delta C_p = 0$ line on the upper wing surface (fig. 9) approaches this optimum location (maximum thickness occurs at the 40-percent chord for this wing). However, because of differences in the flow fields due to camber over the upper and lower surfaces of the wing, the $\Delta C_p = 0$ line on the lower surface is located forward of the $\Delta C_p = 0$ line on the upper surface.

Effect of angle of attack.- Figure 11 shows contours of ΔC_p induced by the symmetrical $M = 1.2$ indentation for $\alpha = 4^\circ$ angle of attack and Mach numbers of 1.125 and 1.43. Only small differences are noted in the strength of the pressure fields at 0° and 4° angle of attack. The main effect is the further displacement of the $\Delta C_p = 0$ lines, and consequently the pressure fields, on the upper and lower surfaces of the wing. This displacement results in a small redistribution of the lift on the wing and body.

Effect of asymmetrical indentation.- The asymmetrical M = 1.4 indentation was designed specifically to produce a redistribution of lift. The pressure fields induced on the upper and lower surfaces of the wing by this asymmetrical indentation are shown in figure 12 for 4° angle of attack and a Mach number of 1.43. The induced pressures shown are those which resulted from changing the symmetrical M = 1.4 indentation to an asymmetrical indentation. It should be mentioned that the total cross-section area distribution for the two configurations are different (see ref. 6). However, it is felt that the differences are not of sufficient magnitude to obscure the effects of asymmetrical indentation. The asymmetrical indentation produced an expansion on the upper surface and a compression on the lower surface over the forward portion of the body and a compression on the upper surface and an expansion on the lower surface over the rearward portion of the body. The compression field on the lower surface of the asymmetrical indentation is relatively weak and is actually ineffective in producing lift. The result of the asymmetry on the induced pressure fields is to increase the lift over the forward regions of the wing and to decrease it over the rearward regions. This redistribution of lift will be shown subsequently to have a favorable effect on the wave drag due to lift.

Drag Analysis for $\alpha = 0^\circ$

Spanwise distribution of drag.- The spanwise variations of section drag loading coefficient for the wing in the presence of the basic and symmetrical M = 1.2 bodies for several Mach numbers and for the symmetrical and asymmetrical M = 1.4 bodies for a Mach number of 1.43 are presented in figure 13. The symmetrical M = 1.2 indentation reduced the drag loading near the wing-root juncture at all Mach numbers. At Mach numbers of 0.94 and 0.98 body indentation increased the drag of the outboard sections. This adverse effect was due to the forward location of the compression field at the low Mach numbers. With increase in Mach number the reduction in drag loading increased in spanwise extent as the induced pressure fields associated with the change in body shape were swept back across the wing. However, the major drag reduction generally occurred over the inboard 60 percent of the semispan. The symmetrical M = 1.4 body, which was cylindrical in the region of the wing, reduced the drag of the wing but was not so effective as the M = 1.2 indentation. A further, but small, reduction in drag loading was obtained when the body was indented asymmetrically. The average drag loading over the bodies at subsonic speeds was lower than the drag loading of the wing near the wing-body juncture; but, it became considerably higher at supersonic speeds.

All the data which have been discussed up to this point are for transition fixed on the wing and body. The pressure distribution over the wing and body for a Mach number of 1.43 with transition natural and

with transition fixed are compared in figure 3 for the basic and symmetrical M = 1.2 bodies. Fixing transition on the wing generally increased the leading-edge pressure coefficient at 0° angle of attack. Figure 12 shows that this increase in leading-edge pressure caused a drag increase over the inboard regions of the wing.

Integrated pressure drag for wing and body.- The pressure drag for the wing has been obtained by integrating the section drag loading between the wing-body juncture and the wing tip, and the drag for the body by performing the integration indicated in the section entitled "Method of Analysis." The variation of the wing pressure drag, body pressure drag, wing-body pressure drag, and skin-friction drag with Mach number are presented in figure 14 for the basic and symmetrical M = 1.2 bodies with fixed transition. Body indentation had no effect on the drag of the wing for Mach numbers below 0.94. Above this Mach number, indentation was effective in reducing the drag at all Mach numbers. The drag for the M = 1.2 body was higher at a Mach number of 0.80 than that for the basic body. The drag-rise Mach number for the indented body was delayed and the drag rise reduced at all Mach numbers except in the region of 1.43. For the wing-body combination body indentation increased the drag at subsonic speeds and reduced the drag rise at all Mach numbers tested. The values of the wing pressure drag, the body pressure drag, and the wing-body drag for a Mach number of 1.43 are listed in the following table for all four configurations with transition fixed and for the basic and symmetrical M = 1.2 wing-body combinations with transition natural:

	Transition fixed				Transition natural	
	Basic body	Symmetrical M = 1.2 body	Symmetrical M = 1.4 body	Asymmetrical M = 1.4 body	Basic body	Symmetrical M = 1.2 body
$C_{D,p,W}$	0.0077	0.0056	0.0070	0.0055	0.0071	0.0051
$C_{D,p,B}$	.0035	.0036	.0031	.0047	.0028	.0031
$C_{D,p,WB}$	.0112	.0092	.0101	.0112	.0099	.0082
$C_{D,f}$	.0066	.0078	------	------	.0071	.0063

For the asymmetrical M = 1.4 body, the drag of the wing, as discussed previously, is reduced. However, it can be seen from the preceding table, that the drag of the body is higher than that of any of the other bodies. As a result, the asymmetrical M = 1.4 wing-body combination has a drag which is higher than that of the symmetrical

$M = 1.4$ wing-body combination and is equal to that of the basic wing-body combination. The effect of transition on the distribution of wing section drag at a Mach number of 1.43 has been discussed previously. With fixed transition, the drag for the wing increased for both the basic and symmetrical $M = 1.2$ wing-body combinations. The drag for the bodies increased also (see preceding table). The net result is an increase in drag of approximately 13 percent.

Skin-friction drag.- The variation of skin-friction drag with Mach number (fig. 14) for both the basic and symmetrical $M = 1.2$ wing-body combinations with transition fixed was obtained from the pressure data obtained in this investigation and the force test results of reference 6. The skin-friction drag for the basic wing-body combination decreased sharply with increase in Mach number at transonic speeds and increased slightly at supersonic speeds. The drag for the wing—indented-body combination was lower at low subsonic speeds than that for the wing—basic-body combination; but, with increase in speed, the skin-friction drag for the indented wing-body combination was higher. These effects of body shape on the friction drag, although generally small, must be assumed to be due to the influence of the induced pressure fields on the boundary layer. At a Mach number of 1.43, fixing transition had only a small effect on the wing—basic-body combination but produced a large increase in skin-friction drag for the wing—indented-body combination (see table given in preceding section). It is evident on the basis of these results that in obtaining the pressure drag rise from force data, the assumption of a constant skin-friction drag at transonic speeds, even for transition fixed, could in some cases lead to erroneous results. For the two wing-body combinations being considered, the drag rise obtained in this manner from the force data indicates no effect of body indentation at a Mach number of 1.43 (ref. 6); actually, the drag rise obtained from pressure data indicates that body indentation produced a considerable reduction in wave drag at this Mach number. For this reason, the calculated drag values that are presented in this paper are, wherever possible, compared with drag values obtained from pressure data.

Comparison of calculated drags with integrated pressure drag.- A comparison of the calculated drags with the integrated pressure drags for the basic and symmetrical $M = 1.2$ body and wing combinations at an angle of attack of 0° is presented in figure 15. The calculated drags consist of the vortex drag, the wave drag due to thickness, and the wave drag due to lift. Values of these various drag components were obtained in the manner described in the section entitled "Method of Analysis."

For both wing-body combinations at subsonic speeds ($M \leq 0.90$) the calculated vortex drag underestimates the integrated pressure drag. At transonic speeds ($0.94 \leq M \leq 1.125$) the sum of the calculated drags does

not adequately predict the integrated pressure drag for either wing-body combination. This result is not suprising since both the wave drag due to thickness and the wave drag due to lift were calculated by means of linearized supersonic theory which does not apply at speeds close to sonic velocity.

At the supersonic Mach number of 1.43, the sum of the calculated drags for the basic body and wing combination is only 0.0004 lower than the integrated pressure drag. For the same Mach number, the sum of the calculated drags for the symmetrical $M = 1.2$ body and wing combination is 0.0015 lower than the integrated pressure drag. A large portion of this error might well be attributed to the inadequate prediction of the vortex drag, which is evident at the subsonic Mach numbers and probably extends throughout the Mach number range.

In the section entitled "Method of Analysis" it was stated that the supersonic wave drag is a function of the axial distribution of $S''(x) - (\beta l'/2q)$. For a symmetrical nonlifting wing-body combination, the contribution of the $\beta l'/2q$ term is usually small enough to be neglected, as it is in the supersonic area rule. In the case of the cambered wing of this paper, however, this term is not negligible even when the net lift is zero. Therefore, the wave drag due to lift has been calculated and included in the comparisons of figure 15. For both the basic and symmetrical $M = 1.2$ body and wing combinations the distribution of $\beta l/2q$ at 0° angle of attack and a Mach number of 1.43 is presented in figure 16 for $\theta = 0^\circ$ and 45°.

The effect of symmetrically indenting the basic body and wing combination for a design Mach number of 1.2 is shown in figure 15(c). The symbols indicate the difference in pressure drag between the basic and symmetrical $M = 1.2$ body and wing combinations. The solid line represents the difference between the total calculated drags of the two combinations. The calculated values predict the effects of indentation within $\Delta C_D = 0.0011$ at Mach numbers of 1.125 and 1.43. It is interesting to note that the effect of indentation is predicted with reasonable accuracy throughout the Mach number range from 1.0 to 1.43, whereas the absolute values of the pressure drag are not predicted with the same degree of accuracy at Mach numbers of 1.125 and below.

Approximate method for determining wave drag due to camber and body asymmetry.- The suggestion is made in reference 4 that the effect of wing camber can be taken into account in the supersonic area rule by considering the wing-chord plane as a reflection plane and treating separately the area distributions above and below this plane. This procedure is based on the consideration of a wing with an attached leading-edge shock wave, so that there is no communication between the upper and lower surface flow fields. Unfortunately, this condition is not satisfied by

the wing-body combinations of this paper since, even at $M = 1.43$, the wing leading edge is swept behind the Mach line. However, in reference 12 it is shown that wings with subsonic leading edges can exert a powerful effect as a divider plate. Therefore, it appears instructive to determine the value of this method for predicting the increment in wave drag due to asymmetry about the wing-chord plane. The question arises as to whether this method will give the same result in practice as would accounting for the camber by including the $\beta l/2q$ term.

A comparison of the slope of the area distribution due to camber (as determined by the method of ref. 4) and $-\beta l/2q$ is presented in figure 17. Also shown is a modification of the method of reference 4. The modification is obtained by multiplying the slope of the area distribution due to camber by $\cos \theta$. This step makes the analogy between the method of reference 4 and the theory of reference 5 more complete since the lift distributions $\beta l/2q$ are multiplied by $\cos \theta$ in order to obtain the component of force in the θ-direction. In determining $S'(x)_{camber}$ an allowance has been made for a small amount of aeroelastic wing twist by an approximate method that will be discussed subsequently.

Comparison of the curves (fig. 17) indicates poor agreement between $S'(x)_{camber}$ and $\beta l/2q$. The agreement is not helped by multiplying $S'(x)_{camber}$ by $\cos \theta$. If the flow field over the wing were two-dimensional, that is, if the pressure coefficient at any point were proportional to the slope of the surface at that point, the distribution of $\beta l/2q$ would be correctly predicted by $S'(x)_{camber} \cos \theta$. The flow field is not two-dimensional, however, since the wing is swept behind the leading-edge Mach line and the wing lies within the region of influence of the body.

The wave drag due to camber has been calculated for the wing—basic-body combination at $M = 1.43$ and $\alpha = 0^\circ$ from the lift distributions ($\beta l/2q$) and from the modification of the method of reference 4 ($S'(x)_{camber} \cos \theta$). The resultant drag-coefficient increments are 0.00108 and 0.00025, respectively.

In the case of the asymmetrical $M = 1.4$ body, the drag analysis requires an estimate of the contribution of the body asymmetry to the wave drag at $\alpha = 0^\circ$. If the lift distribution is known, the incremental drag can be calculated from the distributions of $\beta l/2q$. The suggestion is made in reference 4 that the effect of body asymmetry can be accounted for in a manner similar to that used for wing camber.

A comparison of the slope of the area distribution due to wing camber and body asymmetry (as determined by the method of ref. 4) and the

distribution of $\beta l/2q$ is presented in figure 18. Also shown is a modification of the method of reference 4 obtained by multiplying the slope of the area distribution due to wing camber and body asymmetry by cos θ. The reason for this modification was discussed previously.

Figure 18 indicates that neither the method of reference 4 nor the modified method can predict, even approximately, the distribution of $\beta l/2q$ for a wing-body configuration on which the area is distributed asymmetrically about the wing-chord plane. The values of wave drag due to lift calculated from the distribution of $\beta l/2q$ and the modified method are 0.00058 and 0.00047, respectively.

Drag Analysis for $\alpha = 4^\circ$

Spanwise distribution of drag.- The chordwise pressure distributions presented in reference 7 have been integrated along the wing-section thickness to obtain the section chord force. This chord force, and the section normal forces listed in reference 7 were resolved about the wind axes to obtain a section drag coefficient. Because of the flexibility of this wing, appreciable wing twist due to aeroelastic effects occurred at low angles of attack. The spanwise distribution of wing twist was calculated using the influence coefficients and aerodynamic loads presented in reference 7. These calculated twist angles were then used in resolving the forces about the wind axes.

The spanwise variation of the wing-section drag loading coefficient, $c_d \frac{c}{c_{av}}$, is shown in figure 19 for Mach numbers of 1.03, 1.125, and 1.43, for the wing in the presence of a basic and a symmetrical M = 1.2 indented body. Similar distributions are shown for the symmetrical and asymmetrical M = 1.4 indented bodies at a Mach number of 1.43. The symmetrical M = 1.2 indentation reduced the drag loading over the wing at Mach numbers of 1.03 and 1.125. At a Mach number of 1.43, however, the drag loading near the wing-body juncture is reduced; but, since the pressure field induced by the indentation is swept back sharply, the drag loadings for the outboard wing sections are increased. Both the symmetrical and asymmetrical M = 1.4 indentations redistributed the drag loading over the wing, and caused relatively large increases over the midspan. The drag for the asymmetrical indentation was lower over the inboard 75 percent of the wing semispan than it was for the symmetrical indentation.

Integrated pressure drag for wing and body.- At subsonic speeds, the body drag was increased when the basic body was indented symmetrically for a Mach number of 1.2 (fig. 20); however, substantial reductions occurred at supersonic speeds. The reduction in drag on the body due to the indentation generally was greater than that for 0° angle of attack

and can be attributed to a favorable interaction of the pressures induced on the body by the wing and the body slopes. For the asymmetrical indentation, this interaction was unfavorable and the drag of the body increased as shown in the following table for $M = 1.43$:

	Basic body	Symmetrical $M = 1.2$ body	Symmetrical $M = 1.4$ body	Asymmetrical $M = 1.4$ body
$C_{D,p,W}$	0.0180	0.0177	0.0176	0.0164
$C_{D,p,B}$	.0055	.0050	.0056	.0066
$C_{D,p,WB}$	.0235	.0227	.0232	.0230

The drag of the wing was reduced at all Mach numbers when the wing was in the presence of the symmetrical $M = 1.2$ indented body. However, because the $\Delta C_p = 0$ line is swept back farther along the wing at angle of attack, the reduction in wing drag at 4° angle of attack was considerably less than it was for 0° angle of attack. For the asymmetrical $M = 1.4$ indentation, the $C_p = 0$ line is located farther forward on the wing and the preceding table shows that the largest drag reduction for the wing at a Mach number of 1.43 occurred for the wing in the presence of the asymmetrical $M = 1.4$ indented body.

Because of the reduction in effectiveness of body indentation on the wing drag, the total drag reduction due to indentation was generally smaller at 4° angle of attack than it was at 0° angle of attack (figs. 14 and 20). The drags for the basic and symmetrical $M = 1.2$ combinations as obtained from the pressure data also are compared in figure 20 with the force test results of reference 6. Because of differences in rigidity of the two wings, the incremental drag between the two sets of data included not only skin-friction drag but also drag differences due to aeroelastic wing twist.

Vortex drag.- The spanwise load distributions at several Mach numbers for the wing-body combinations with the basic and symmetrical $M = 1.2$ bodies are presented in figure 21. Also shown are the spanwise load distributions for the symmetrical and asymmetrical $M = 1.4$ indented body and wing combinations at a Mach number of 1.43. The vortex drag has been calculated from these distributions. The results are presented in figure 22 in terms of the vortex drag due to lift parameter $C_{D,v}/C_L{}^2$. The variation with Mach number is much the same for both the basic and symmetrical $M = 1.2$ body and wing combinations. The value of the vortex drag due to lift parameter varied from 42 to 55 percent

above the value of $1/\pi A$, the value for an elliptic spanwise load distribution. The value of the vortex drag due to lift parameter for the symmetrical $M = 1.4$ and asymmetrical $M = 1.4$ indented-body and wing combinations are both about 51 percent above the minimum value of $1/\pi A$.

Wave drag due to lift.- The method used in calculating the wave drag due to lift has been dsicussed in the section entitled "Method of Analysis." It is believed, however, that the distributions of $\beta l/2q$ presented in this paper are perhaps the first experimental distributions obtained for a sweptback wing and warrant considerable discussion.

The required distribution of $\beta l/2q$ for the minimum drag due to lift derived from the wave-drag equation of reference 5 is elliptical for all values of θ. A similar conclusion was arrived at by Jones in deriving the minimum drag due to lift for the special case of an elliptical-plan-form wing (ref. 13). The experimental distributions obtained for the 45° sweptback wing—basic-body combination depart greatly from elliptical shapes and vary considerably with θ and with Mach number (fig. 6). For a Mach number of 1.43, the $\theta = 0^\circ$ lift distribution is smooth but builds up rapidly to a sharp peak. With increasing θ, the distributions are elongated along the body axis; however, the peaks of the distributions tend to become more abrupt. The magnitude of the peaks generally decreases with increasing θ because the l/q term is a function of the cosine of the angle θ. With decrease in Mach number, the magnitude of the distributions decreases because of the $\beta = \sqrt{M^2 - 1}$ term. The actual shapes of the distributions also differ because of the effect of Mach number on the cutting plane angle. For $\theta = 0^\circ$, the only effect is in the β term; and, the shapes of the distributions for a constant lift are essentially the same.

The incremental wave drag calculated from the θ-distributions for several body shapes are plotted against θ in figure 23 for Mach numbers of 1.43 and 1.125. The symmetrical $M = 1.2$ indentation, as noted previously, caused a small redistribution of the lift on the wing at angles of attack. Thus, although the wave drag due to lift is independent of the thickness drag, the redistribution of lift caused by indenting the body to obtain a reduction in thickness wave drag can influence the wave drag due to lift. Indentation, at a Mach number of 1.125, caused a small reduction in the peaks and a small increase over the forward portion of the $\beta l/2q$ distributions for the wing—basic-body combination (fig. 5). These changes in the $\beta l/2q$ distributions were favorable and, as indicated in figure 23, reduced the wave drag due to lift. With increase in Mach number to 1.43, the induced pressure fields on the upper surface of the wing are swept back sharply (see fig. 10) and the additional lift which results tends to aggravate the peaks of the $\beta l/2q$ distributions and increase the drag. The asymmetrical $M = 1.4$ indentation was designed specifically to alter the lift distribution of the

wing. The peaks of the $\beta l/2q$ distributions for both θ cuts were reduced by the asymmetrical indentation and a substantial drag reduction occurred.

The parameter for wave drag due to lift $C_{D,w}/C_L^2$ for the wing—basic-body combination is compared in the following table with the parameter calculated for the symmetrical $M = 1.2$ and the asymmetrical $M = 1.4$ indented body and wing combinations.

Mach number	Basic body	Symmetrical $M = 1.2$ body	Asymmetrical $M = 1.4$ body	Lower bound
1.03	0.0089	0.0087	------	0.00473
1.125	.0413	.0381	------	.0152
1.43	.1590	.1454	0.1134	.0588

Also shown in the table is the parameter for wave drag due to lift calculated for a wing-body combination which would have distributions of the same length as the experimental wing body but which had elliptical shapes. The drag for this hypothetical wing-body combination may be considered as representing a lower bound for the wave drag due to lift. It should be kept in mind that the minimum wave drag that can be achieved for a particular plan form wing and body combination may be higher than the lower bound.

Comparison of calculated drags with integrated pressure drag.- A comparison of the sums of the calculated drags with the integrated pressure drags for the basic and symmetrical $M = 1.2$ body and wing combinations at an angle of attack of 4° is presented in figure 24. The calculated drags are the vortex drag, the wave drag due to thickness, and the wave drag due to lift. Each of these drag components has been discussed previously.

For both wing-body combinations at subsonic speeds ($M \leq 0.94$) the vortex drag computed from the spanwise load distributions underestimates the integrated pressure drag by 6 to 13 percent. At transonic speeds ($0.94 < M \leq 1.125$) the sum of the calculated drags does not adequately predict the integrated pressure drag for either wing-body combination. As was the case for an angle of attack of 0°, agreement was not expected since both the wave drag due to thickness and the wave drag due to lift were calculated by means of linearized supersonic theory which does not apply at speeds close to sonic velocity.

At the supersonic Mach number of 1.43, the sum of the calculated drags for the basic body and wing combination is approximately 8 percent higher than that for the integrated pressure drag. For this same Mach number, the sum of the calculated drags for the symmetrical $M = 1.2$ body and wing combination is less than 1 percent below the integrated pressure drag. The sum of the calculated drags for the asymmetrical $M = 1.4$ body and wing combination is 0.0214 compared with the integrated pressure drag which is 0.0230. The sum of the calculated drags underestimated the integrated pressure drag by approximately 7 percent.

Approximate method for determining distribution of $\beta l/2q$.- In reference 4 the possibility of obtaining wave drag due to wing camber and body asymmetry has been suggested. The method has been modified in this paper in order to obtain a closer analogy between this method and the theory of reference 5. It is now suggested that the modified method might be extended to the case of a wing-body combination at an angle of attack and that an equivalent area distribution due to angle of attack can be found. The angle of attack may be any combination of angle of attack of the body, wing incidence, wing twist, and effective twist due to body induced upwash. The derivation of the equivalent area distribution due to angle of attack is presented in the section entitled "Method of Analysis."

The slope distributions of the areas due to angle of attack are plotted with the distributions of $\beta l/2q$ for the wing—basic-body combination at several Mach numbers in figure 24. The slopes of the areas due to angle of attack have been multiplied by $\beta \cos \theta$ in order to obtain a better comparison with variation in Mach number. These distributions include the effect of aeroelastic wing twist (ref. 7), effective wing twist due to body induced upwash $\left(\alpha_u = \alpha_B \frac{R^2}{y^2}\right.$ as predicted in ref. 14$\left.\right)$, and wing camber (in the manner described previously in this paper).

At a Mach number of 1.03, the distributions of $\beta l/2q$ are predicted, within reasonable limits, by the negative slopes of the area distributions due to angle of attack $-\beta S'(x)\cos \theta$. At $M = 1.125$ the agreement between $\beta l/2q$ and $-\beta S'(x)\cos \theta$ is quite good for $\theta = 0^\circ$. For $\theta = 45^\circ$, the agreement is generally good except at the peaks ($x \approx 12$) of the distributions. For $M = 1.43$, the agreement for both $\theta = 0^\circ$ and 45° is not too good, particularly toward the rear of the distributions. However, the magnitudes of the peaks and the general shape of the distributions of $\beta l/2q$ are well represented by $-\beta S'(x)\cos \theta$.

Comparisons of $\beta l/2q$ and $-\beta S'(x)\cos\theta$ for the symmetrical $M = 1.2$ and the asymmetrical $M = 1.4$ body and wing combinations at $M = 1.43$ are presented in figure 26. Similar to the basic body and wing combination, the agreement is generally poor, particularly toward the rear of the distributions. Again, however, the general shapes of the $\beta l/2q$ distributions are well represented by $-\beta S'(x)\cos\theta$.

Values of the incremental wave drag due to lift $C_{D,w,\theta}$ have been computed from the distributions of $\beta l/2q$ and $-\beta S'(x)\cos\theta$ in figures 25 and 26 and are presented in figure 27 as a function of θ. The values of wave drag due to lift calculated from $-\beta S'(x)\cos\theta$ generally underestimate the values obtained from $\beta l/2q$. The differences were all within about 7 percent with three exceptions. Two exceptions occurred for the basic body and wing combination, $\theta = 45^\circ$ cuts, at $M = 1.03$ and 1.125. These differences were of the order of 0.0005 and 0.0019, respectively, which represents only 2 and 8 percent of the total calculated drag coefficients presented in figure 23. The third exception occurred for the symmetrical $M = 1.2$ body and wing combination, $\theta = 0^\circ$ cut, at $M = 1.43$. This difference was 0.0041 and represents 18 percent of the total calculated drag coefficient shown in figure 23.

Values of the wave drag due to lift obtained from the curves of figure 26 are presented in the following table. Included in the table are the percent differences between $C_{D,w}$ calculated from $-\beta S'(x)\cos\theta$ and $C_{D,w}$ calculated from $\beta l/2q$ (based on $C_{D,w}$ from $\beta l/2q$). These differences are also presented as percent of total calculated drag.

Configuration	M	$C_{D,w}$		Percent difference	Percent of total calculated drag
		From $\beta l/2q$	From $-\beta S'(x)\cos\theta$		
Basic body	1.03	0.0011	0.0008	27.2	1.3
Basic body	1.125	.0042	.0035	16.7	2.8
Basic body	1.43	.0090	.0083	7.8	2.8
Symmetrical $M = 1.2$ body	1.43	.0093	.0080	14.0	5.8
Asymmetrical $M = 1.4$ body	1.43	.0068	.0066	2.9	.9

The results in this table indicate that although the percent difference between the wave drags due to lift calculated from $-\beta S'(x)\cos\theta$ and $\beta l/2q$ may be large, the errors introduced into the total calculated drag are reasonably small. For the five examples cited herein, these errors are all less than 6 percent. Thus, it appears that the method presented herein of obtaining the wave drag due to lift from the distribution of $-\beta S'(x)\cos\theta$ will afford an estimate of the actual wave drag due to lift without a knowledge of the pressure distribution on the configuration.

CONCLUSIONS

An investigation of effects of body shape on the drag of a 45° swept-back wing-body combination at Mach numbers from 0.90 to 1.43 resulted in the following conclusions:

1. Both the expansion and compression fields induced by body indentation were swept back as the stream Mach number increased from 0.94. The line of zero pressure change was generally tangent to the Mach lines associated with the local velocities over the wing and body.

2. The strength of the induced pressure fields over the wing were attenuated with spanwise distance and the major effects were limited to the inboard 60 percent of the wing semispan.

3. Asymmetrical body indentation tended to increase the lift on the forward portion of the wing and reduce the lift on the rearward portion. This redistribution of lift had a favorable effect on the wave drag due to lift.

4. Symmetrical body indentation reduced the drag loading near the wing-body juncture at all Mach numbers. The reduction in drag loading increased in spanwise extent as the Mach number increased and the line of zero induced pressure became more nearly alined with the line of maximum wing thickness. However, the major drag reduction generally occurred over the inboard 60 percent of the semispan.

5. Calculations of the wave drag due to thickness, the wave drag due to lift, and the vortex drag of the basic and symmetrical $M = 1.2$ body and wing combinations at an angle of attack of 0° predicted the effects of indentation within 11 percent of the wing-basic body drag throughout the Mach number range from 1.0 to 1.43. However, the absolute values of the pressure drag were not predicted with the same degree of accuracy at Mach numbers of 1.125 and below.

6. Neither the method based upon the reflection of disturbances by the wing nor a modification of the method suggested in this paper successfully predicted the distribution of the oblique-section lift parameter $\beta l/2q$ for a wing-body configuration on which the area is distributed asymmetrically about the wing-chord plane. Consequently, these methods appear to be of little value in predicting the incremental wave drag due to lift resulting from wing camber and/or body asymmetry for a wing with subsonic leading edges.

7. Calculations of the wave drag due to thickness, the wave drag due to lift, and the vortex drag for the basic, symmetrical $M = 1.2$, and asymmetrical $M = 1.4$ body and wing combinations predicted the total pressure drag to within 8 percent of the experimental value at $M = 1.43$. At Mach numbers of 1.125 and 1.03, the predictions were not so accurate. The incremental pressure drag due to a symmetrical $M = 1.2$ indentation was predicted to within 8 percent of the total pressure drag of the wing—indented-body combination for all Mach numbers investigated above 1.0.

8. A modification and extension of the method based upon the reflection of disturbances by the wing to the case of a wing-body combination at an angle of attack of 4° proved useful in predicting the distributions of $\beta l/2q$. The differences in wave drag due to lift calculated from the predicted and experimental distributions of $\beta l/2q$ were less than 6 percent of the total pressure drag.

Langley Research Center,
National Aeronautics and Space Administration,
Langley Field, Va., Aug. 1, 1958.

REFERENCES

1. Whitcomb, Richard T.: A Study of the Zero-Lift Drag-Rise Characteristics of Wing-Body Combinations Near the Speed of Sound. NACA Rep. 1273, 1956. (Supersedes NACA RM L52H08.)

2. Whitcomb, Richard T., and Fischetti, Thomas L.: Development of a Supersonic Area Rule and an Application to the Design of a Wing-Body Combination Having High Lift-to-Drag Ratios. NACA RM L53H31a, 1953.

3. Jones, Robert T.: Theory of Wing-Body Drag at Supersonic Speeds. NACA Rep. 1284, 1956. (Supersedes NACA RM A53H18a.)

4. Whitcomb, Richard T.: Some Considerations Regarding the Application of the Supersonic Area Rule to the Design of Airplane Fuselages. NACA RM L56E23a, 1956.

5. Lomax, Harvard: The Wave Drag of Arbitrary Configurations in Linearized Flow As Determined by Areas and Forces in Oblique Planes. NACA RM A55A18, 1955.

6. Loving, Donald L.: A Transonic Investigation of Changing Indentation Design Mach Number on the Aerodynamic Characteristics of a 45° Sweptback-Wing—Body Combination Designed for High Performance. NACA RM L55J07, 1956.

7. Fischetti, Thomas L.: Investigation at Mach Numbers From 0.8 to 1.43 of Pressure and Load Distributions Over a Thin 45° Sweptback Highly Tapered Wing in Combination With Basic and Indented Bodies. NACA RM L57D29a, 1957.

8. Matthews, Clarence W.: An Investigation of the Adaptation of a Transonic Slotted Tunnel to Supersonic Operation by Enclosing the Slots With Fairings. NACA RM L55H15, 1955.

9. Cahn, Maurice S., and Olstad, Walter B.: A Numerical Method for Evaluating Wave Drag. NACA TN 4258, 1958.

10. Heaslet, Max A., and Lomax, Harvard: Supersonic and Transonic Small Perturbation Theory. General Theory of High Speed Aerodynamics. Vol. VI of High Speed Aerodynamics and Jet Propulsion, sec. D., W. R. Sears, ed., Princeton Univ. Press, 1954, pp. 122-344.

11. McLean, F. Edward, and Rennemann, Conrad, Jr : Supersonic Flow Past Nonlifting Bumped and Indented Bodies of Revolution. NACA TN 3744, 1956.

12. Hall, James Rudyard: Two Experiments on Applications of the Transonic Area Rule to Asymmetric Configurations. NACA RM L56A25, 1956.

13. Jones, Robert T.: Theoretical Determination of the Minimum Drag of Airfoils at Supersonic Speeds. Jour. Aero. Sci. vol. 19, no. 12, Dec. 1952, pp. 813-822.

14. Beskin, L.: Determination of Upwash Around a Body of Revolution at Supersonic Velocities. CVAC-DEVF Memo BB-6, APL/JHU-CM-251, The Johns Hopkins Univ., Appl. Phys. Lab., May 27, 1946.

TABLE I.- BODY ORDINATES

Body station, x, in.	Radius, in.				
	Basic body	Symmetrical M = 1.2 body	Symmetrical M = 1.4 body	Asymmetrical M = 1.4 body (upper)	Asymmetrical M = 1.4 body (lower)
0	0	0	0	0	0
.5	.165	.165	.165	.165	.165
1.0	.282	.282	.282	.282	.282
1.5	.378	.378	.378	.378	.378
2.0	.460	.460	.460	.460	.460
2.5	.540	.540	.545	.545	.545
3.0	.612	.612	.623	.623	.623
3.5	.680	.680	.693	.693	.693
4.0	.743	.743	.763	.763	.763
4.5	.806	.806	.827	.827	.827
5.0	.862	.862	.890	.890	.890
5.5	.917	.917	.951	.951	.951
6.0	.969	.969	1.009	1.009	1.009
6.5	1.015	1.015	1.063	1.063	1.063
7.0	1.062	1.062	1.114	1.114	1.114
7.5	1.106	1.106	1.166	1.166	1.166
8.0	1.150	1.150	1.215	1.215	1.215
8.5	1.187	1.187	1.262	1.262	1.262
9.0	1.222	1.222	1.307	1.307	1.307
9.5	1.257	1.257	1.352	1.352	1.352
10.0	1.290	1.290	1.396	1.396	1.396
10.5	1.320	1.320	1.438	1.438	1.438
11.0	1.350	1.350	1.480	1.480	1.480
11.5	1.376	1.376	1.519	1.519	1.519
12.0	1.404	1.404	1.555	1.555	1.555
12.5	1.430	1.427	1.579	1.579	1.579
13.0	1.452	1.440	1.586	1.586	1.586
13.5	1.476	1.440	1.586	1.564	1.606
14.0	1.493	1.433	1.586	1.539	1.617
14.5	1.512	1.416	1.586	1.515	1.626
15.0	1.526	1.390	1.586	1.487	1.635
15.5	1.540	1.359	1.586	1.464	1.641
16.0	1.552	1.323	1.586	1.444	1.651
16.5	1.565	1.283	1.586	1.423	1.659
17.0	1.575	1.242	1.586	1.412	1.666
17.5	1.585	1.203	1.586	1.400	1.674
18.0	1.590	1.173	1.586	1.391	1.681

TABLE I.- Concluded

BODY ORDINATES

Body station, x, in.	Radius, in.				
	Basic body	Symmetrical M = 1.2 body	Symmetrical M = 1.4 body (upper)	Asymmetrical M = 1.4 body (upper)	Asymmetrical M = 1.4 body (lower)
18.5	1.598	1.149	1.586	1.388	1.689
19.0	1.602	1.133	1.586	1.390	1.694
19.5	1.606	1.126	1.586	1.400	1.697
20.0	1.606	1.133	1.586	1.427	1.701
20.5	1.604	1.150	1.586	1.469	1.702
21.0	1.602	1.175	1.586	1.507	1.700
21.5	1.600	1.202	1.586	1.536	1.692
22.0	1.594	1.236	1.596	1.555	1.675
22.5	1.587	1.269	1.591	1.568	1.649
23.0	1.578	1.306	1.576	1.573	1.622
23.5	1.570	1.341	1.569	1.568	1.597
24.0	1.560	1.363	1.554	1.555	1.574
24.5	1.547	1.375	1.539	1.539	1.549
25.0	1.532	1.380	1.521	1.521	1.521
25.5	1.517	1.380	1.500	1.500	1.500
26.0	1.501	1.376	1.479	1.479	1.479
26.5	1.480	1.370	1.456	1.456	1.456
27.0	1.460	1.362	1.433	1.433	1.433
27.5	1.438	1.349	1.410	1.410	1.410
28.0	1.414	1.335	1.388	1.388	1.388
28.5	1.387	1.319	1.365	1.365	1.365
29.0	1.360	1.300	1.340	1.340	1.340
29.5	1.330	1.280	1.315	1.315	1.315
30.0	1.300	1.255	1.290	1.290	1.290
30.5	1.269	1.230	1.259	1.259	1.259
31.0	1.231	1.201	1.229	1.229	1.229
31.5	1.193	1.170	1.195	1.195	1.195
32.0	1.158	1.138	1.156	1.156	1.156
32.5	1.118	1.100	1.116	1.116	1.116
33.0	1.076	1.065	1.073	1.073	1.073
33.5	1.030	1.023	1.030	1.030	1.030
34.0	.984	.980	.985	.985	.985
34.5	.936	.933	.934	.934	.934
35.0	.878	.878	.879	.879	.879
35.5	.825	.825	.823	.823	.823
36.0	.762	.762	.767	.767	.767
36.15	.750	.750	.702	.702	.702

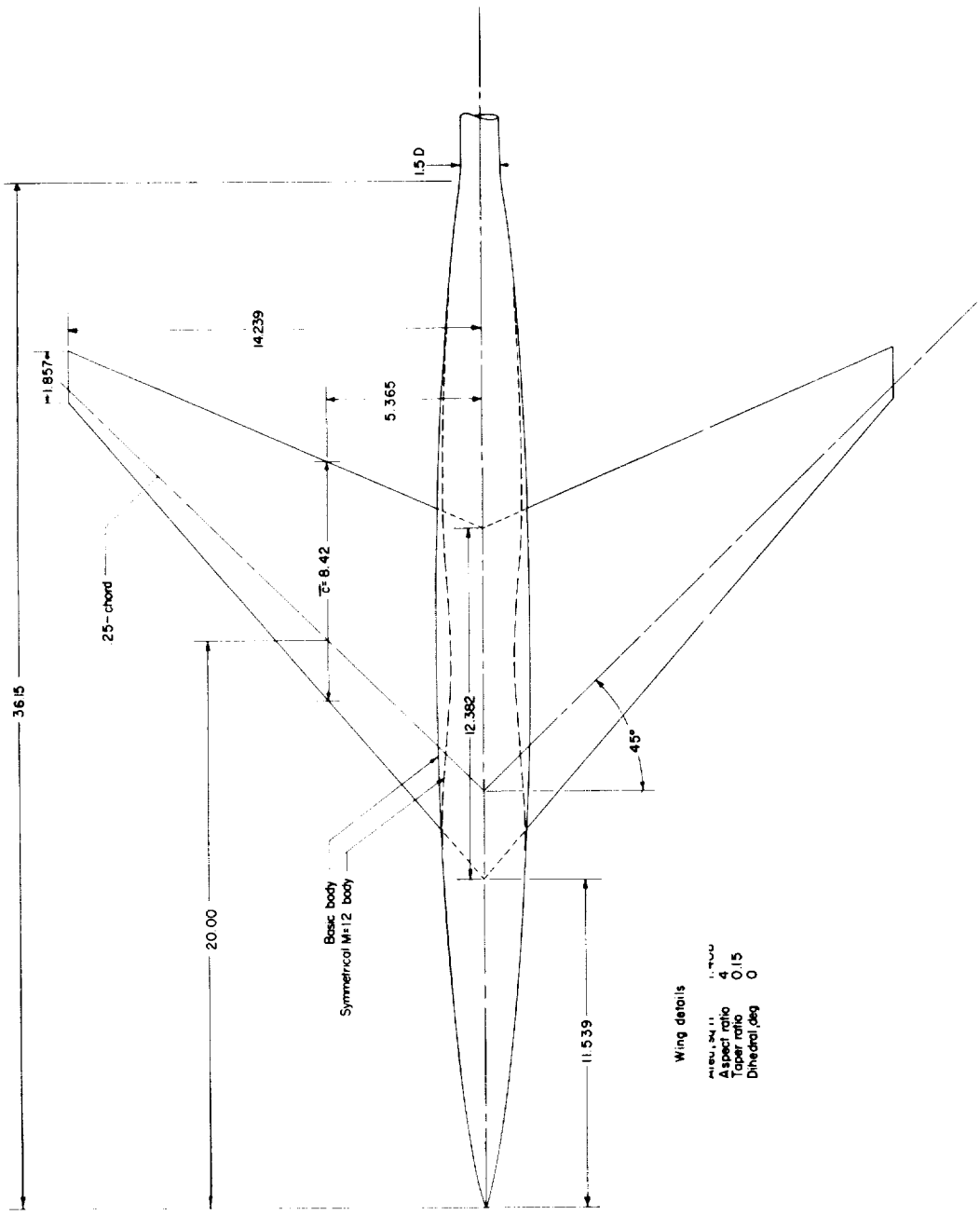

Figure 1.- Details of the wing with the basic Sears-Haack body and a body indented symmetrically for M = 1.2. All dimensions are in inches.

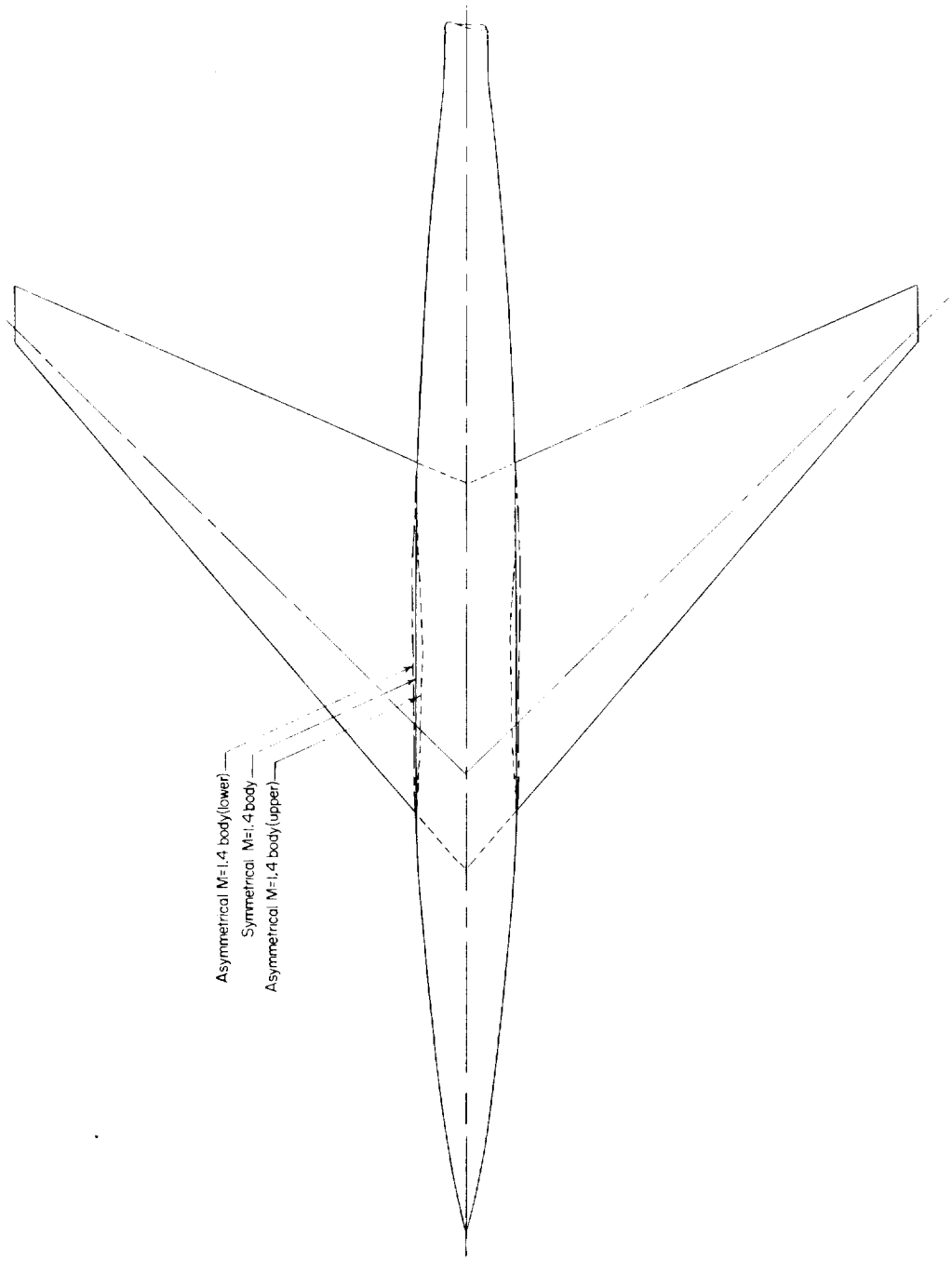

Figure 2.- Sketch of the wing with a symmetrical M = 1.4 and an asymmetrical M = 1.4 indentation.

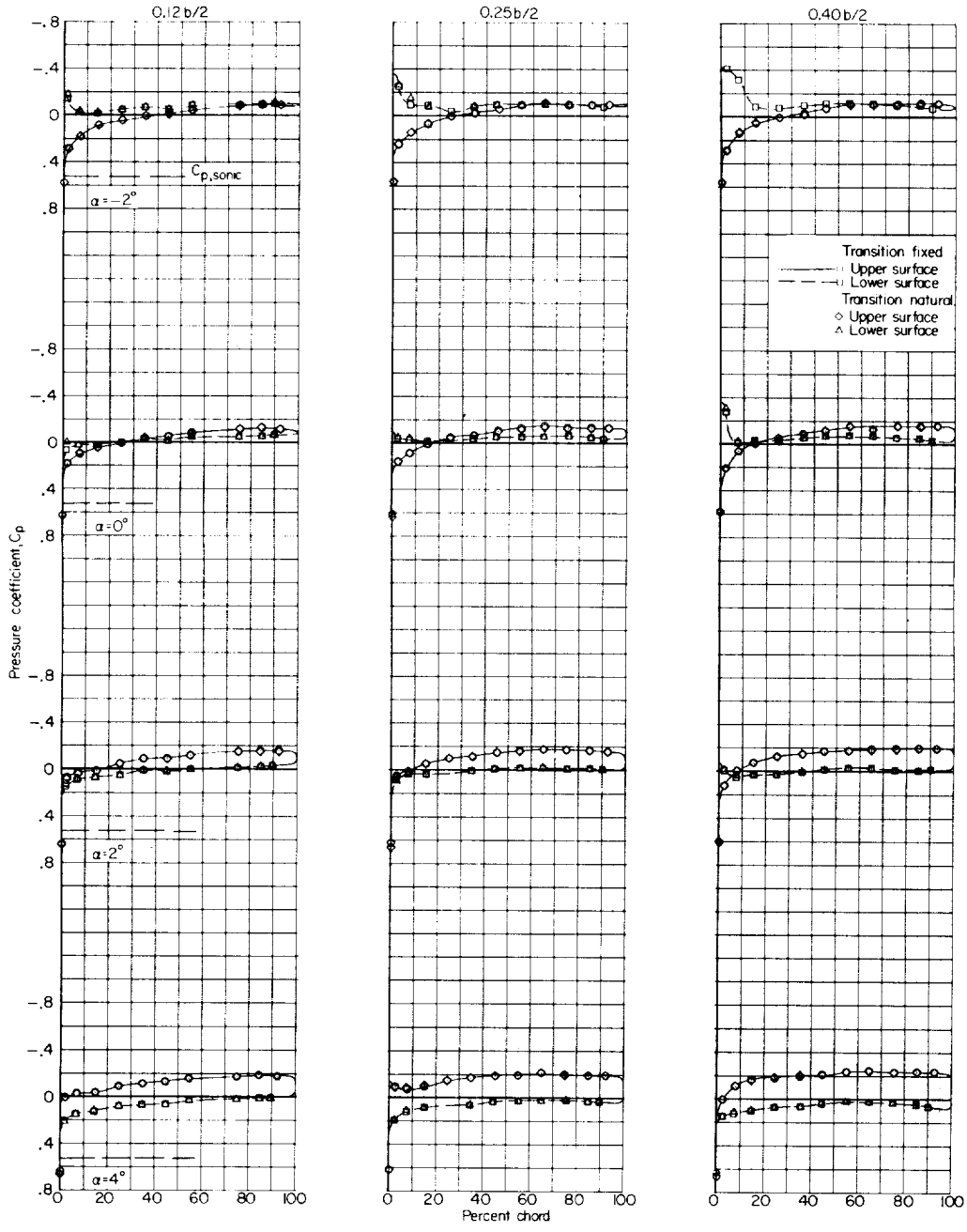

(a) Wing in presence of basic body.

Figure 3.- Pressure distribution at a Mach number of 1.43 for the wing—basic-body combination and the symmetrical M = 1.2 body and wing combination with transition fixed and natural.

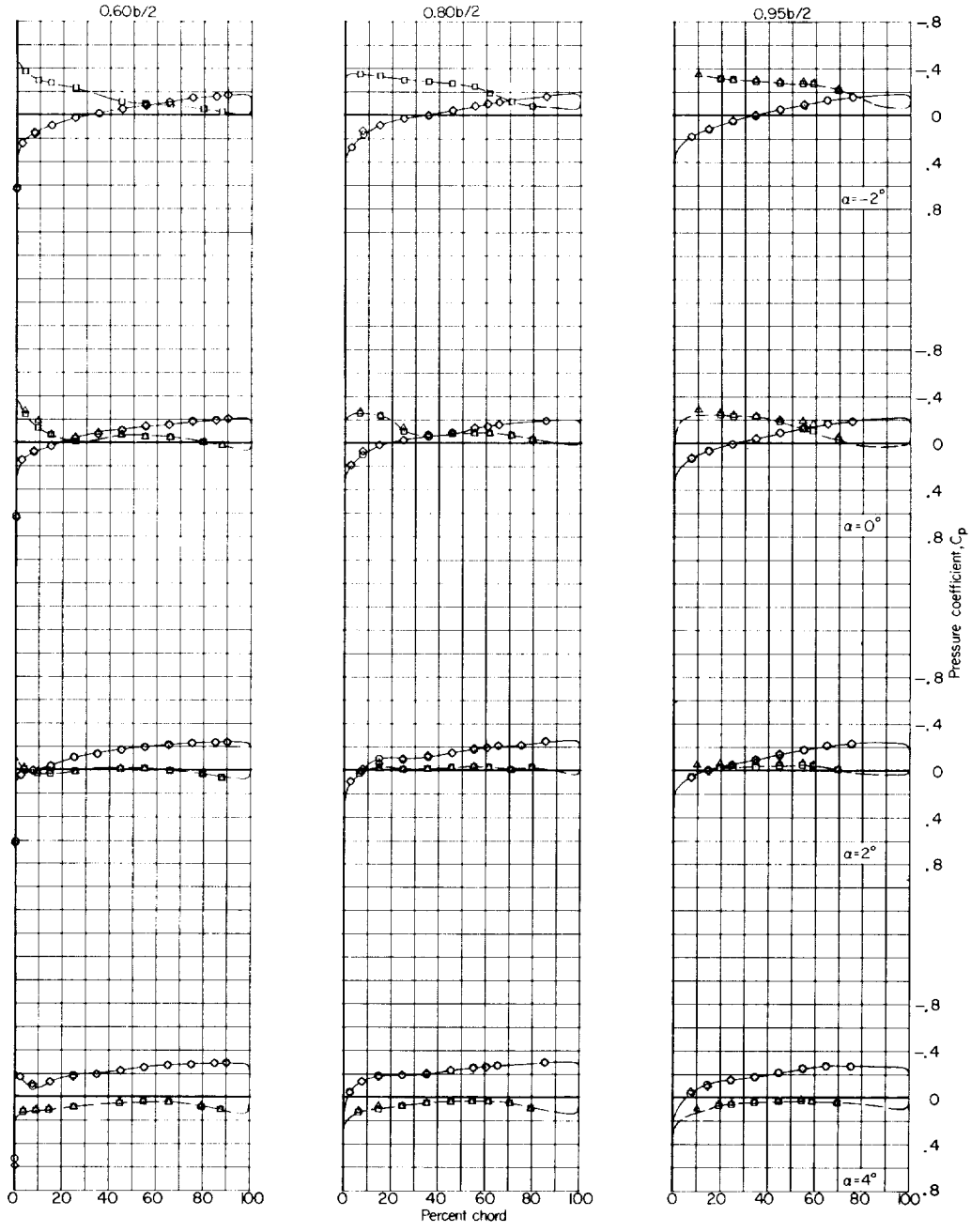

(a) Concluded.

Figure 3.- Continued.

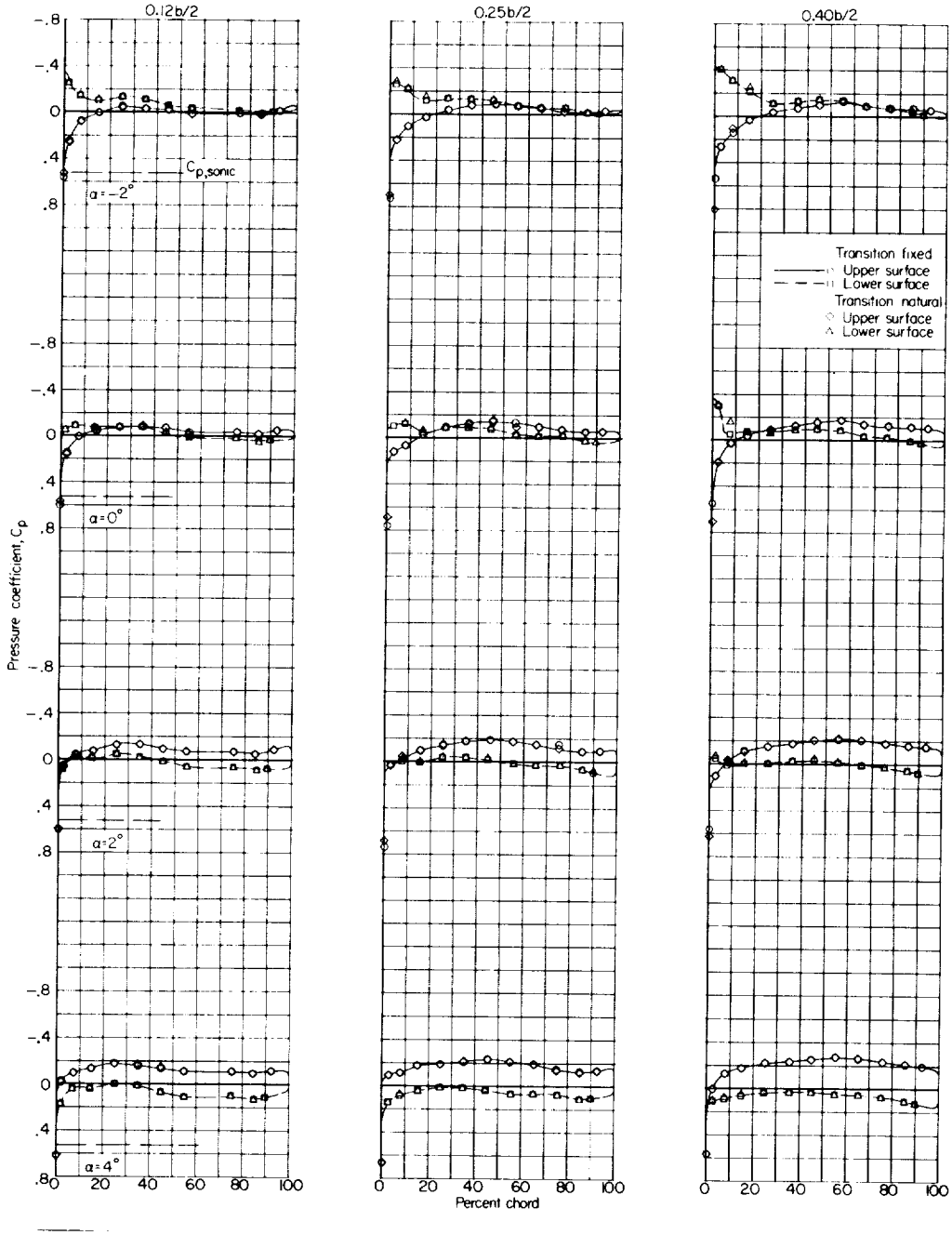

(b) Wing in presence of symmetrical M = 1.2 body.

Figure 3.- Continued.

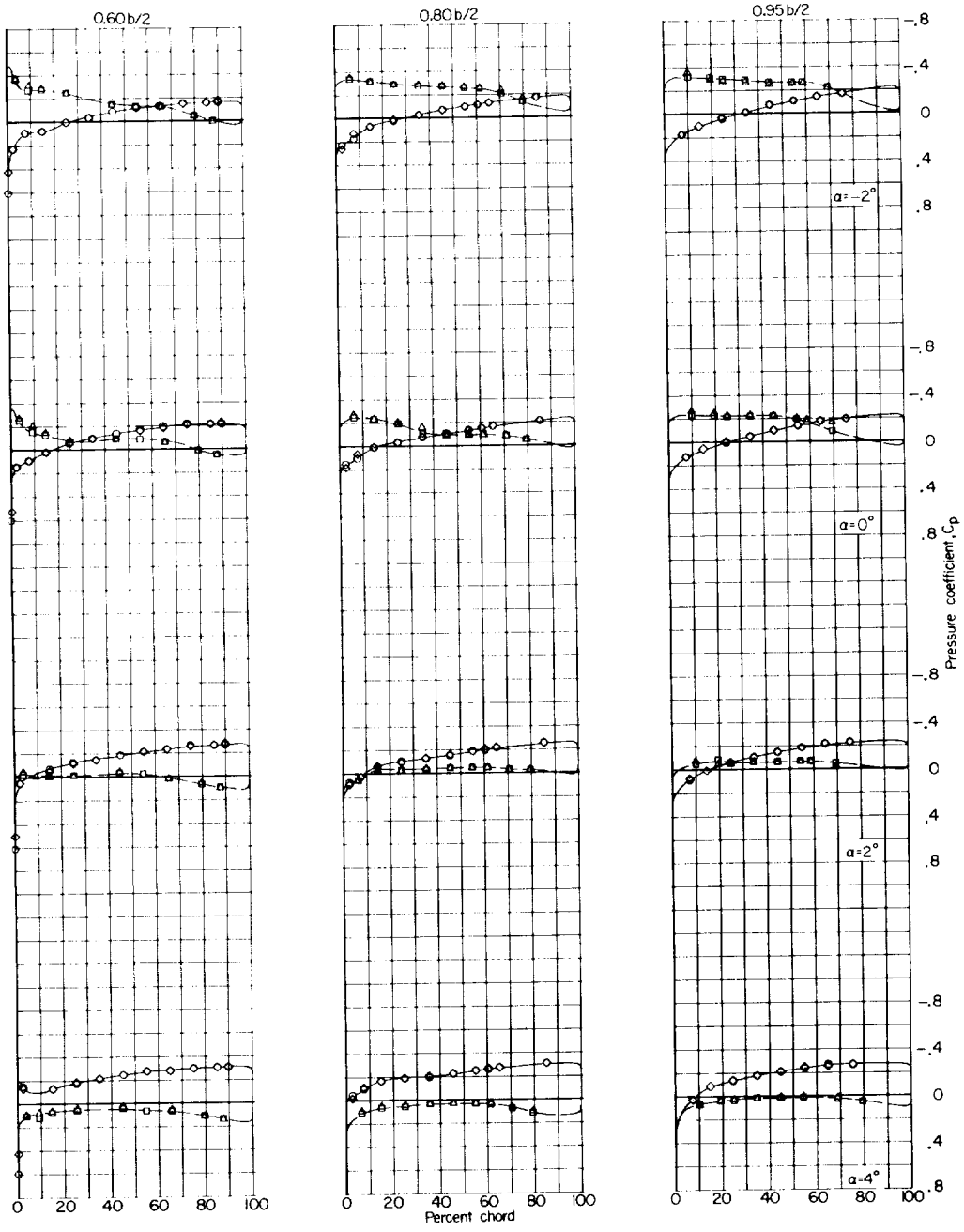

(b) Concluded.

Figure 3.- Continued.

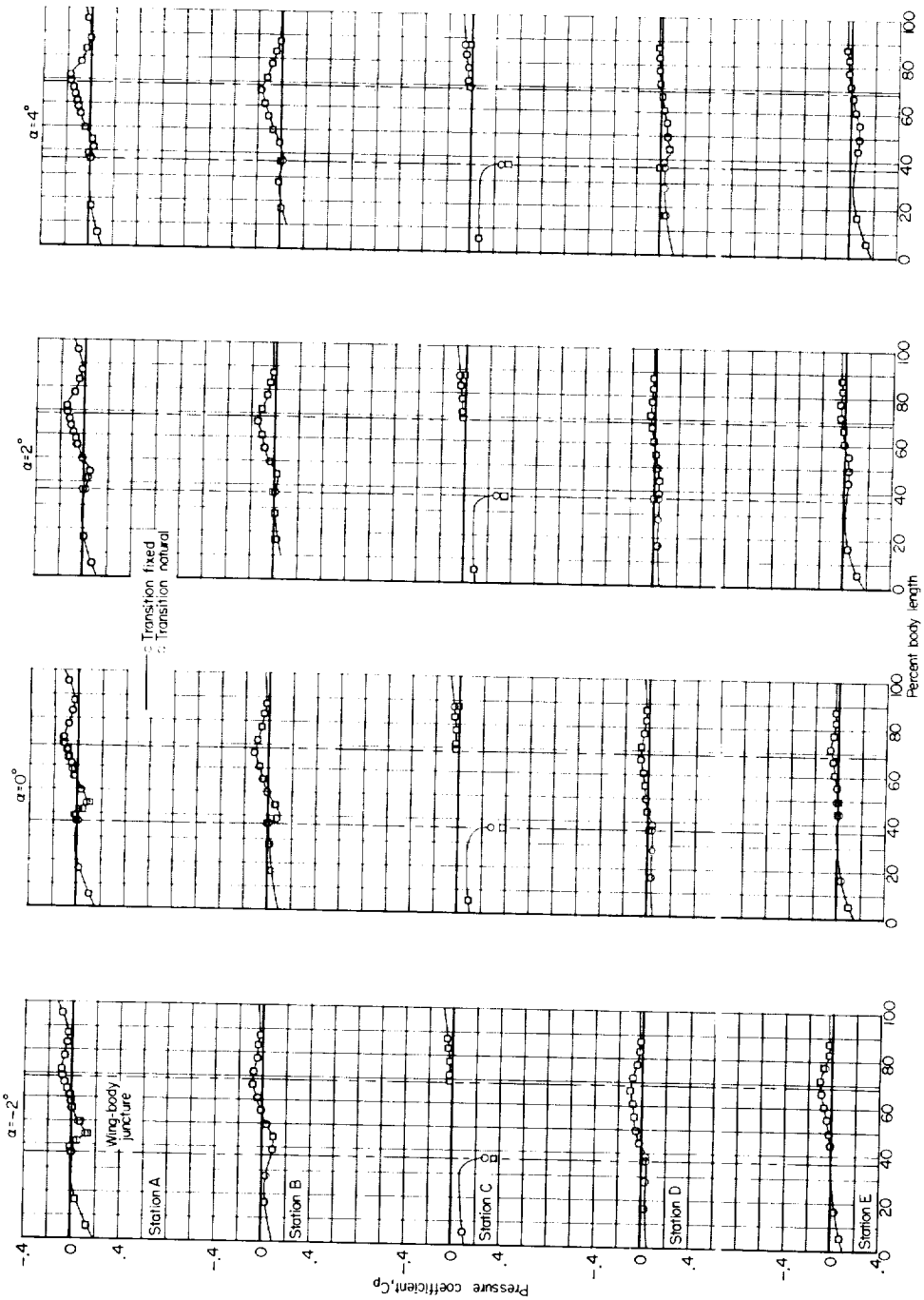

(c) Basic body in presence of wing.

Figure 3.- Continued.

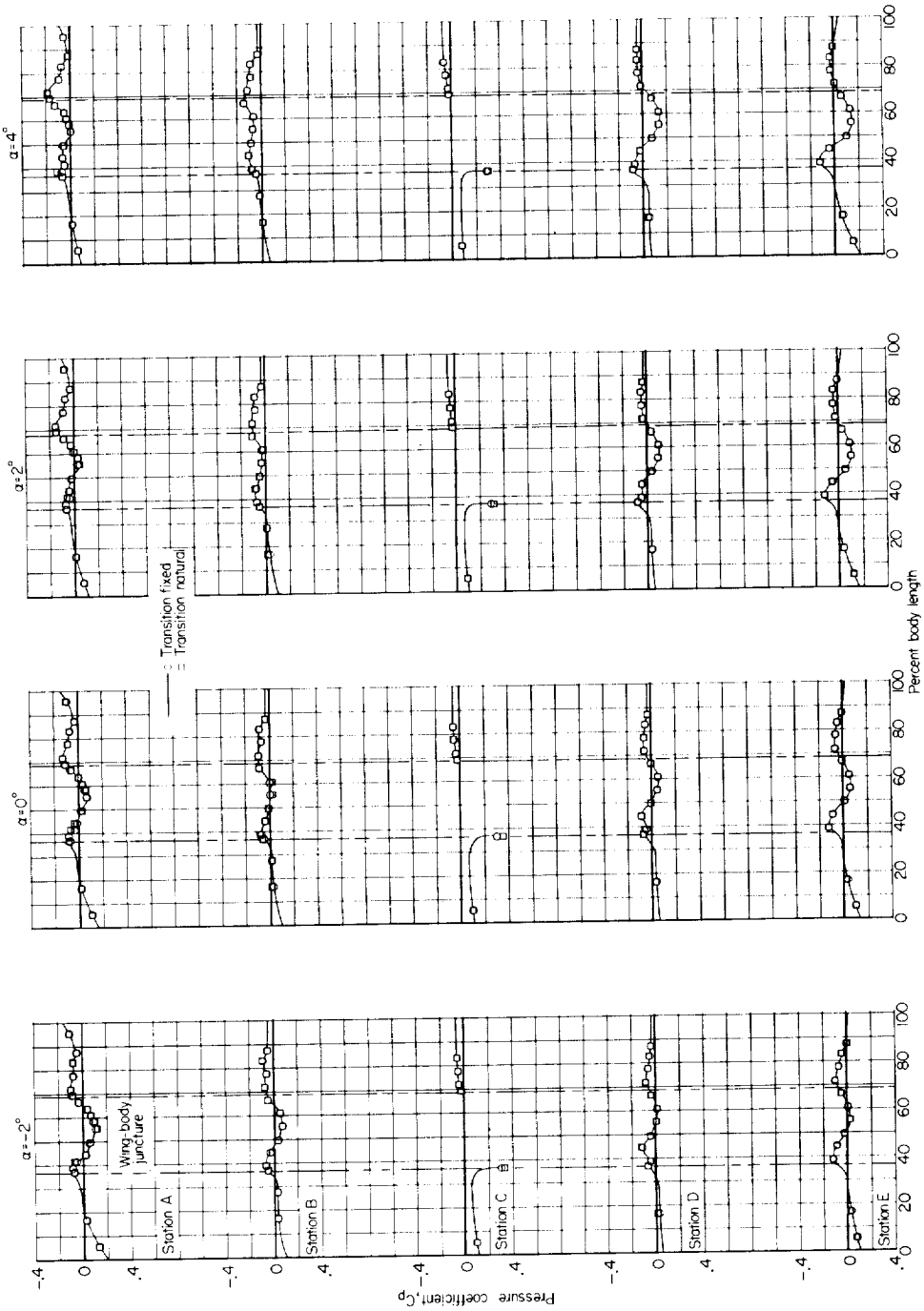

(d) Symmetrical M = 1.2 body in presence of wing.

Figure 3.- Concluded.

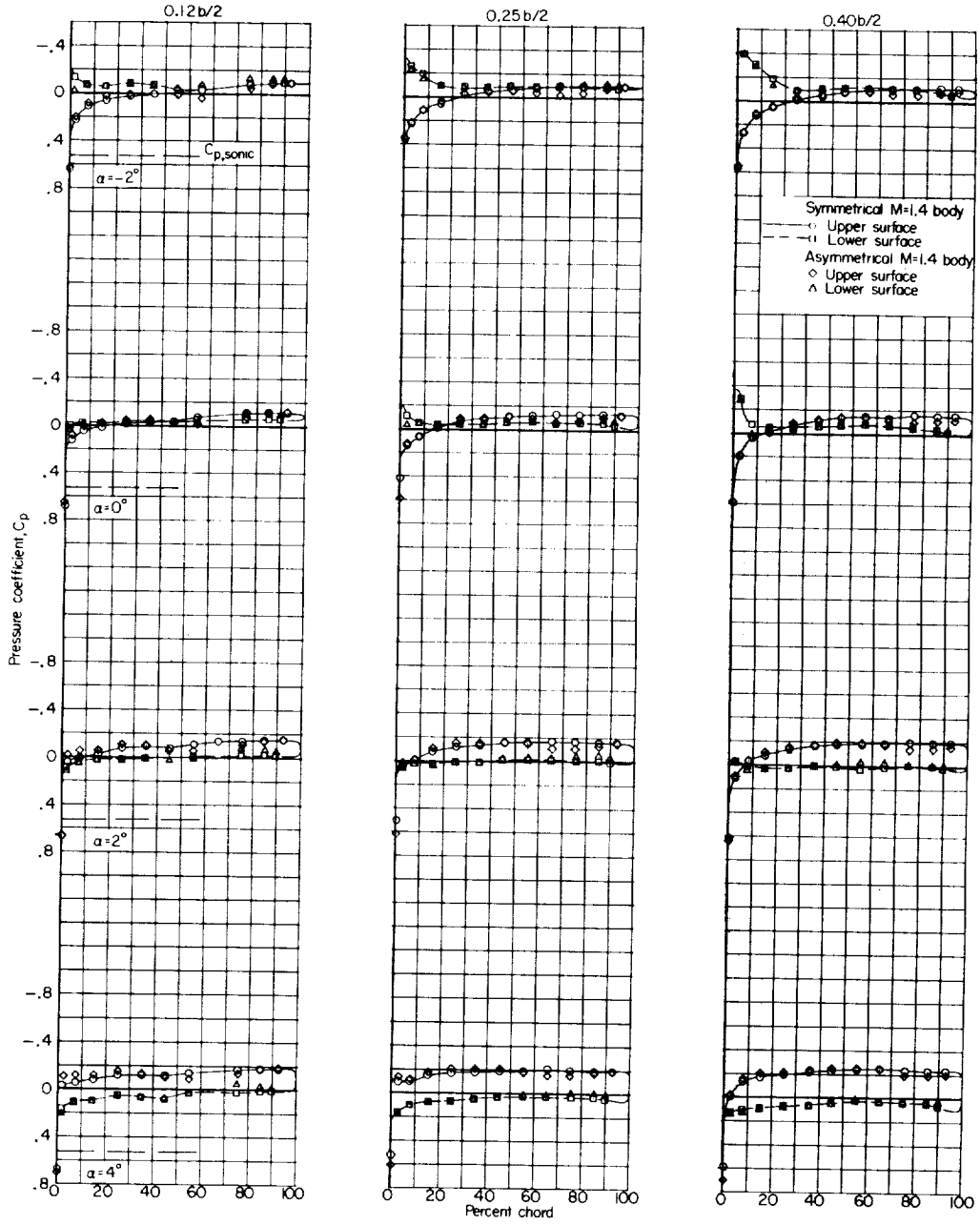

(a) Wing in presence of body

Figure 4.- Pressure distribution at a Mach number of 1.43 for the symmetrical M = 1.4 body and wing combination and the asymmetrical M = 1.4 body and wing combinations. Transition fixed.

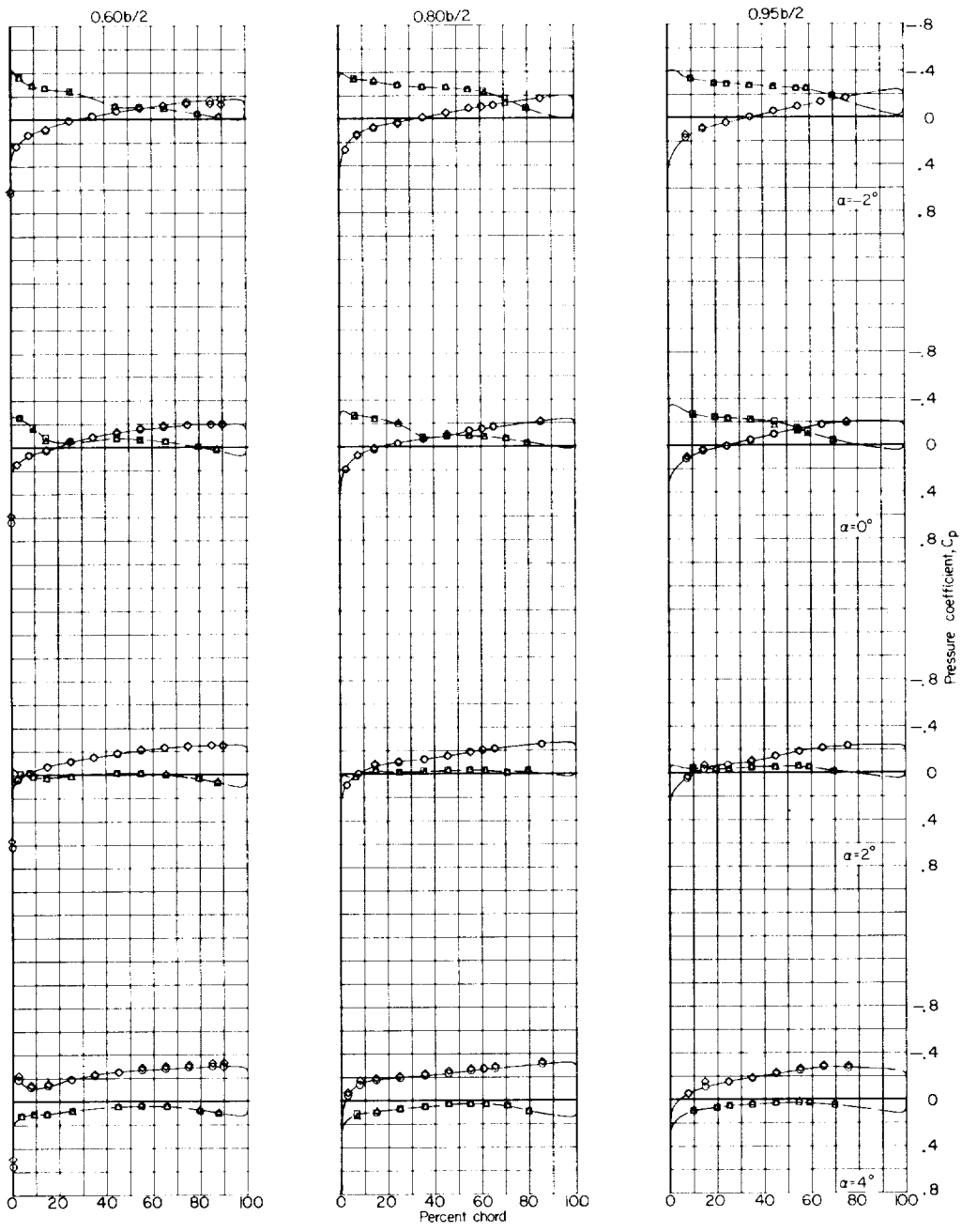

(a) Concluded.

Figure 4.- Continued.

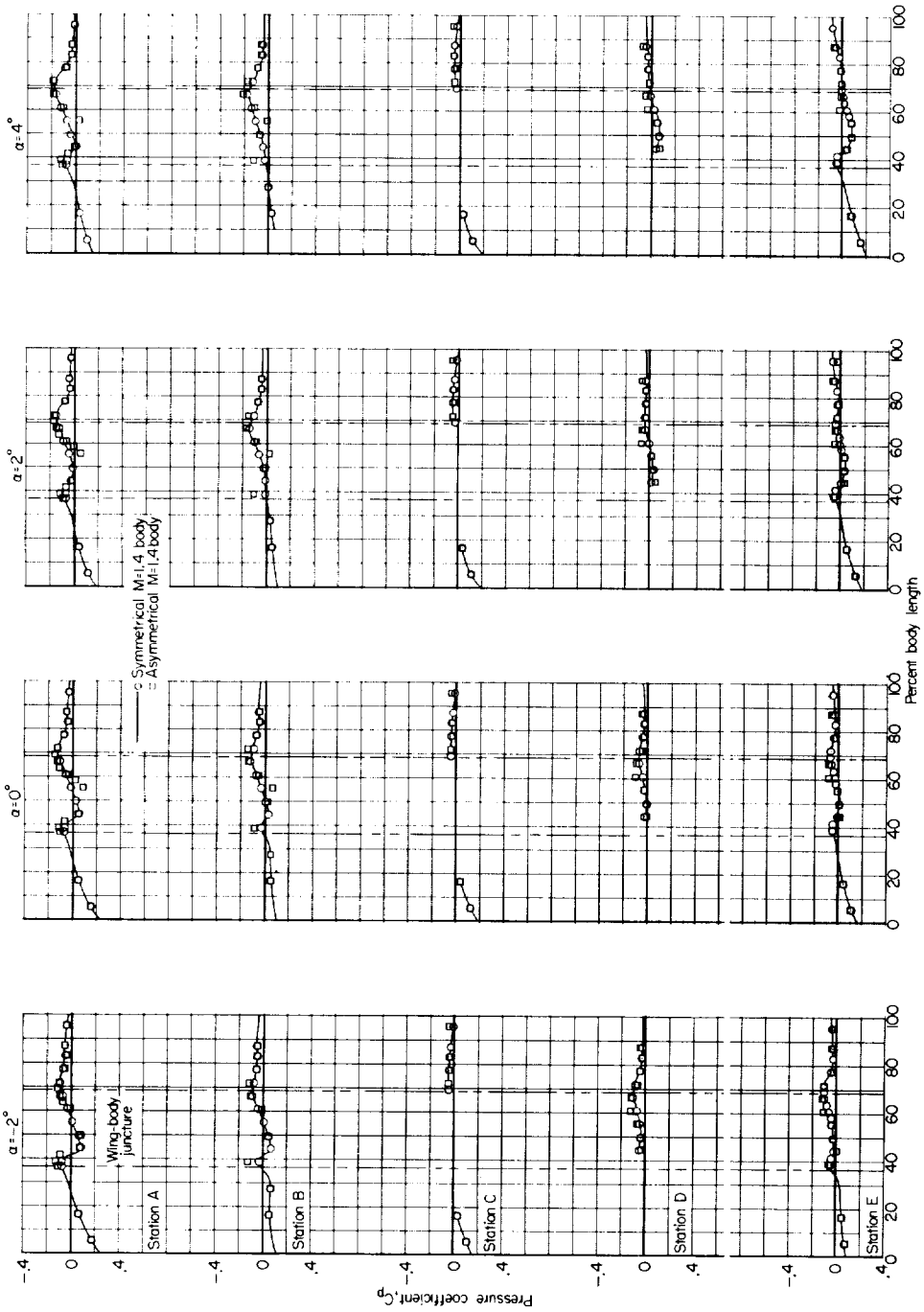

(b) Body in presence of wing.

Figure 4.- Concluded.

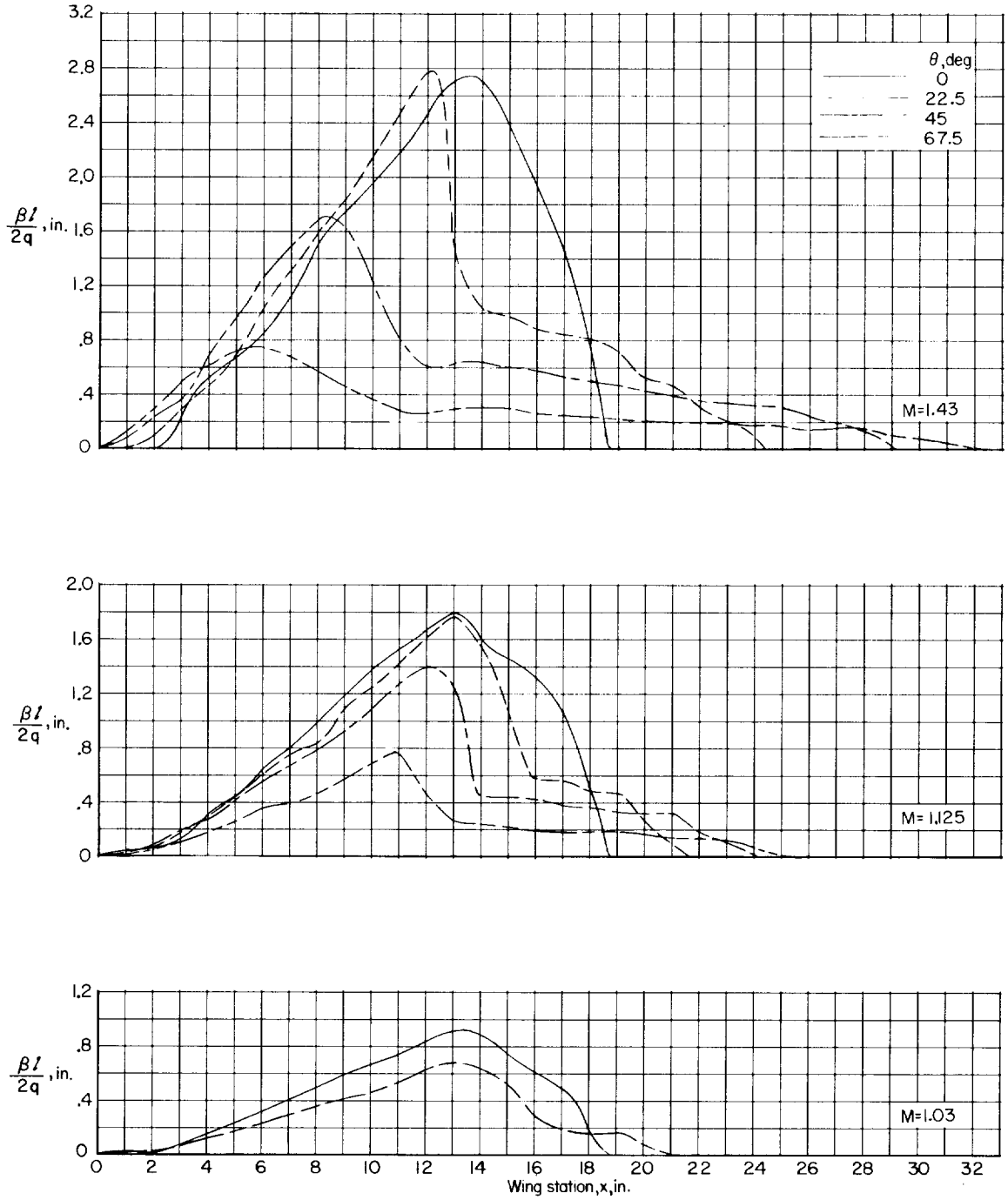

Figure 5.- Distribution of $\beta l/2q$ for the wing—basic-body combination. $\alpha = 4^{\circ}$.

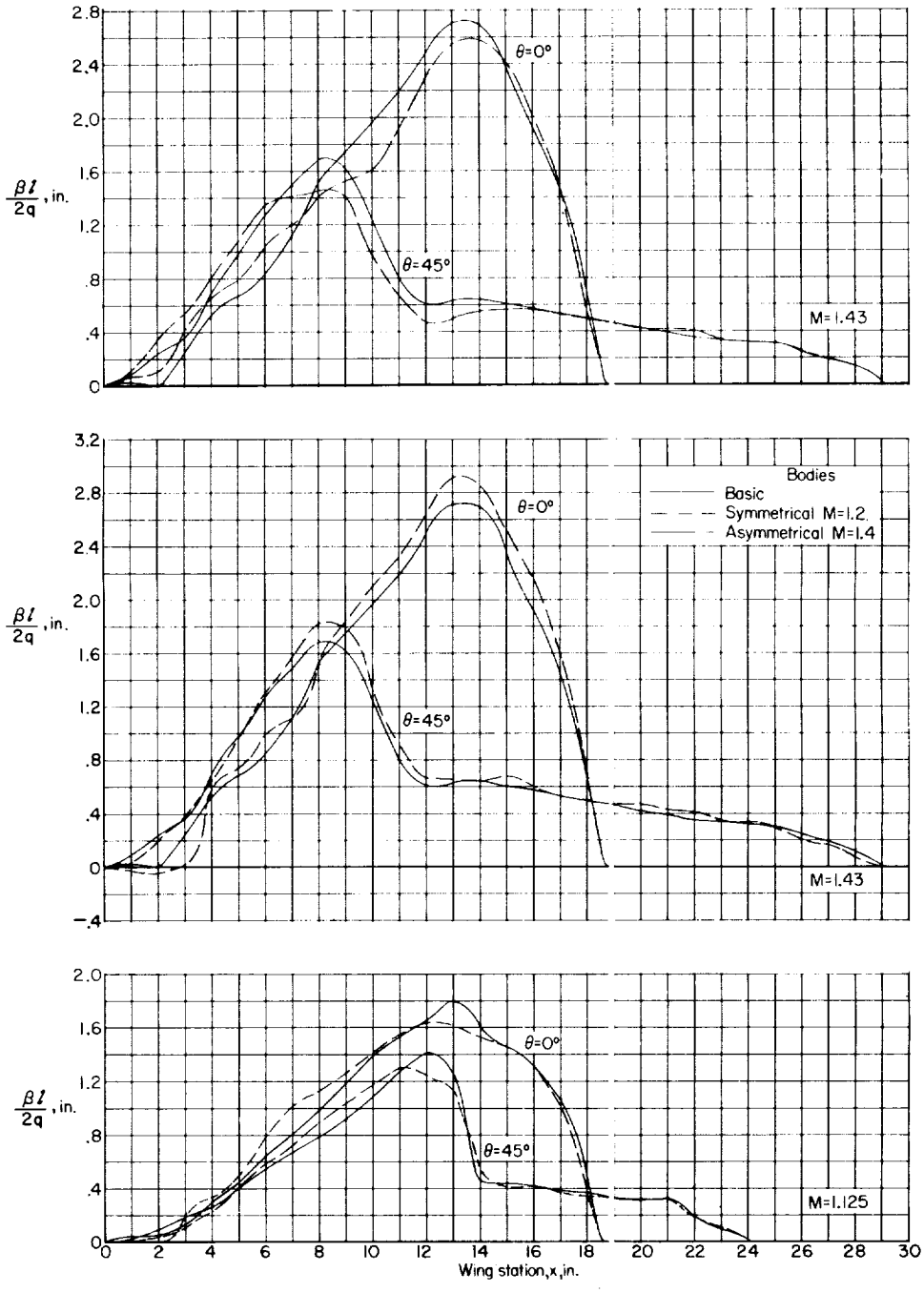

Figure 6.- Effect of body shape on the distribution of $\beta l/2q$. $\alpha = 4^{o}$.

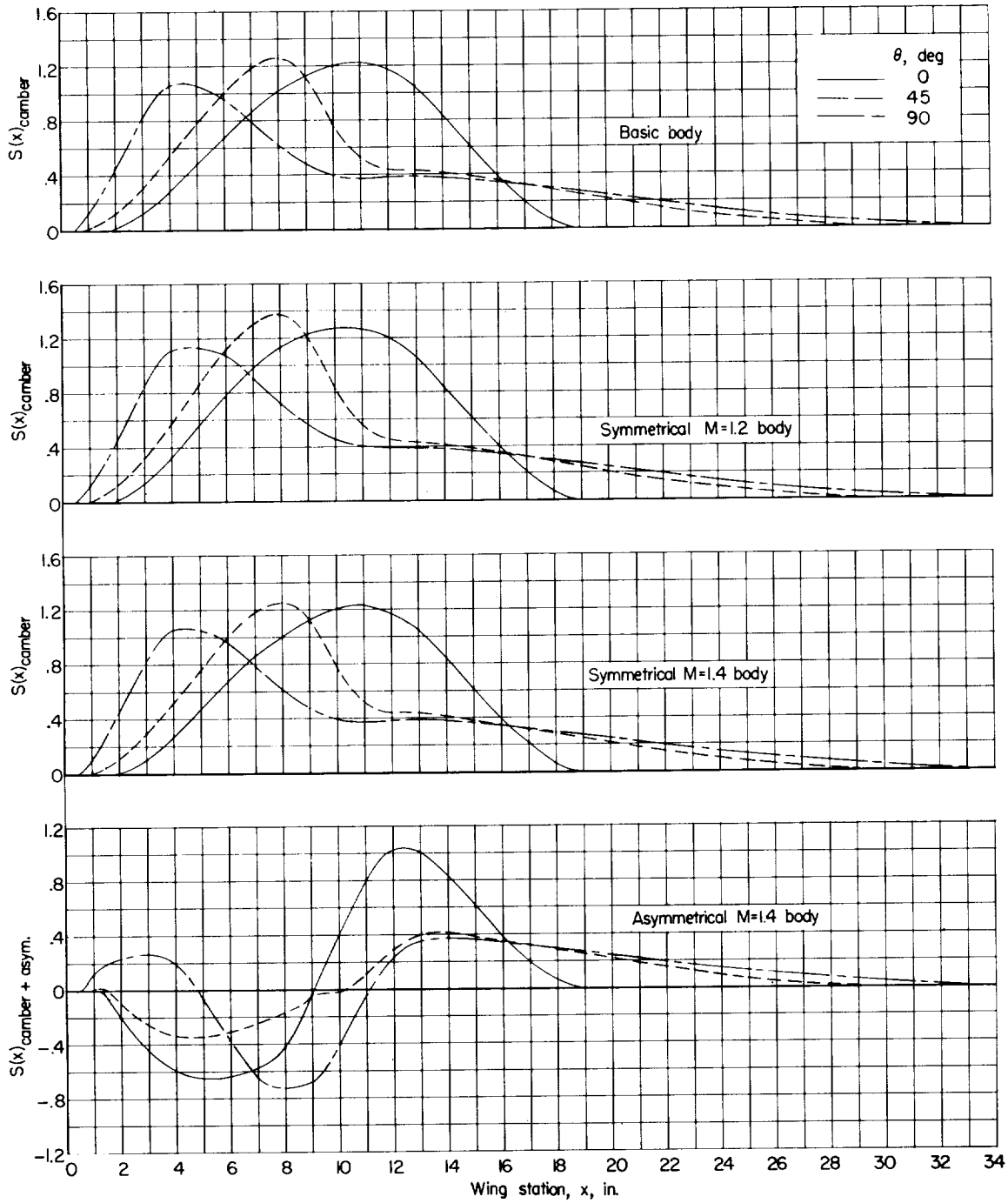

Figure 7.- Distribution of cross-sectional area due to wing camber and body asymmetry at M = 1.4.

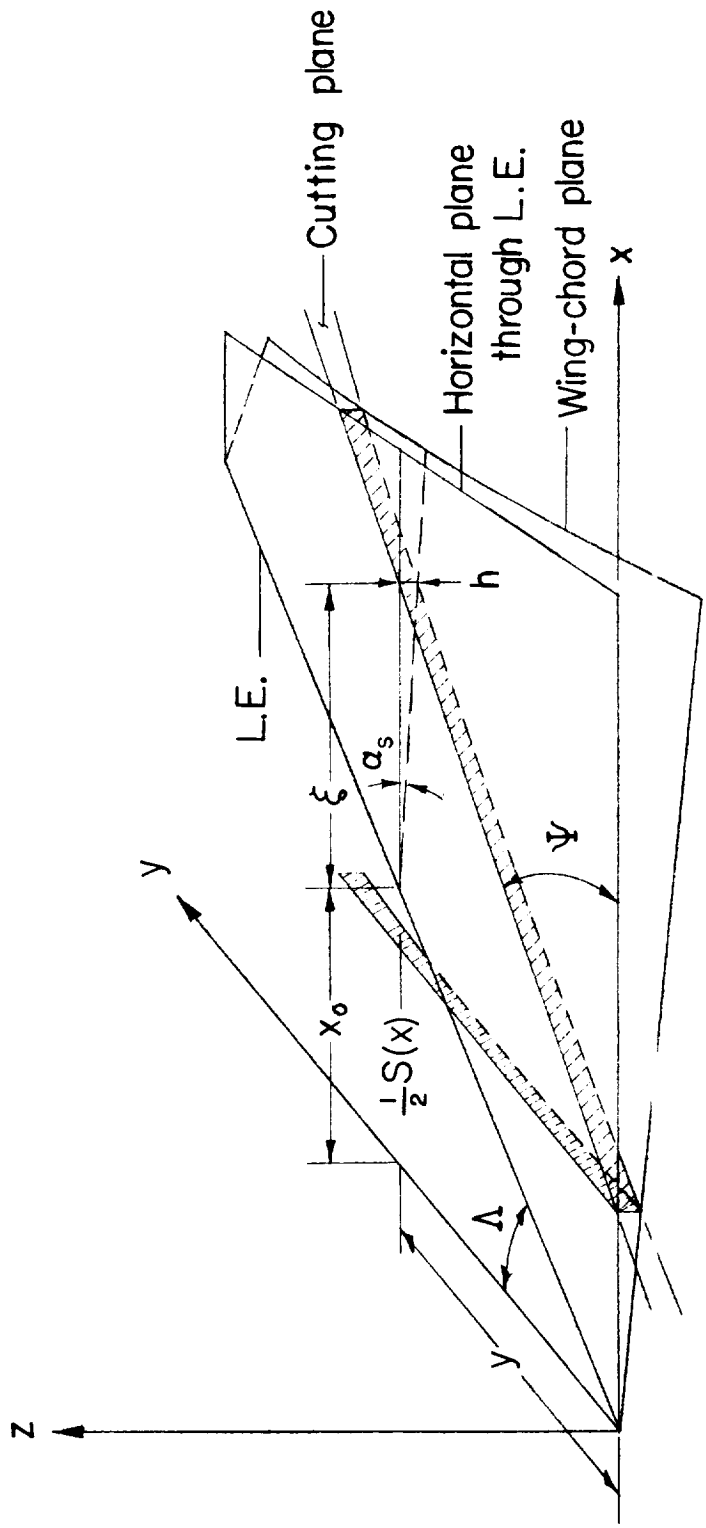

Figure 8.- Sketch of the cross-sectional area due to angle of attack of the wing-chord plane.

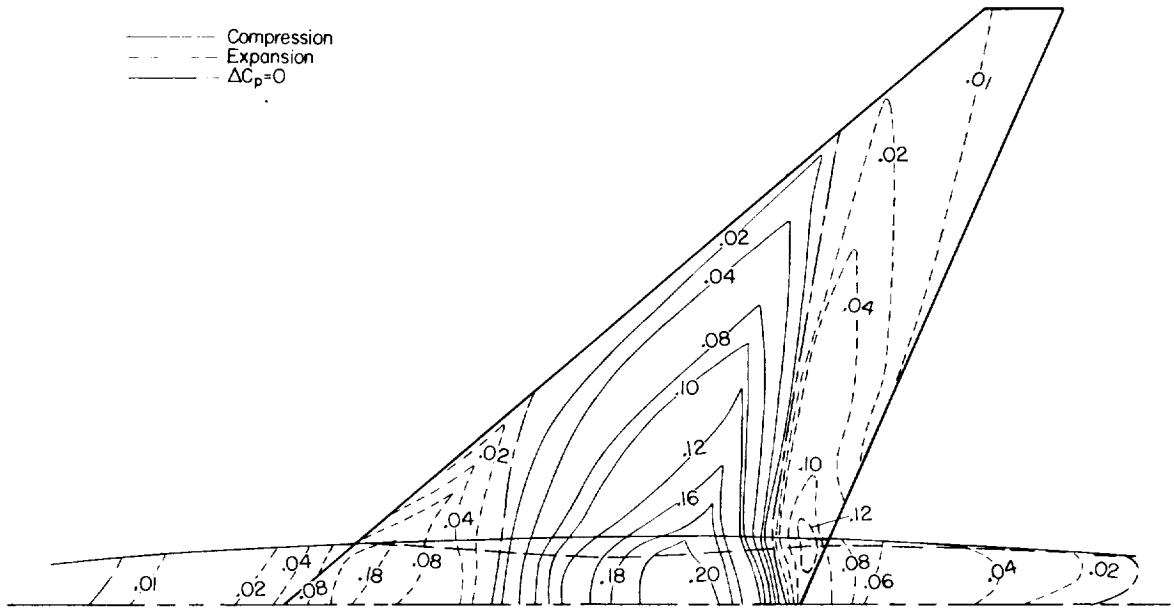

(a) M = 0.94.

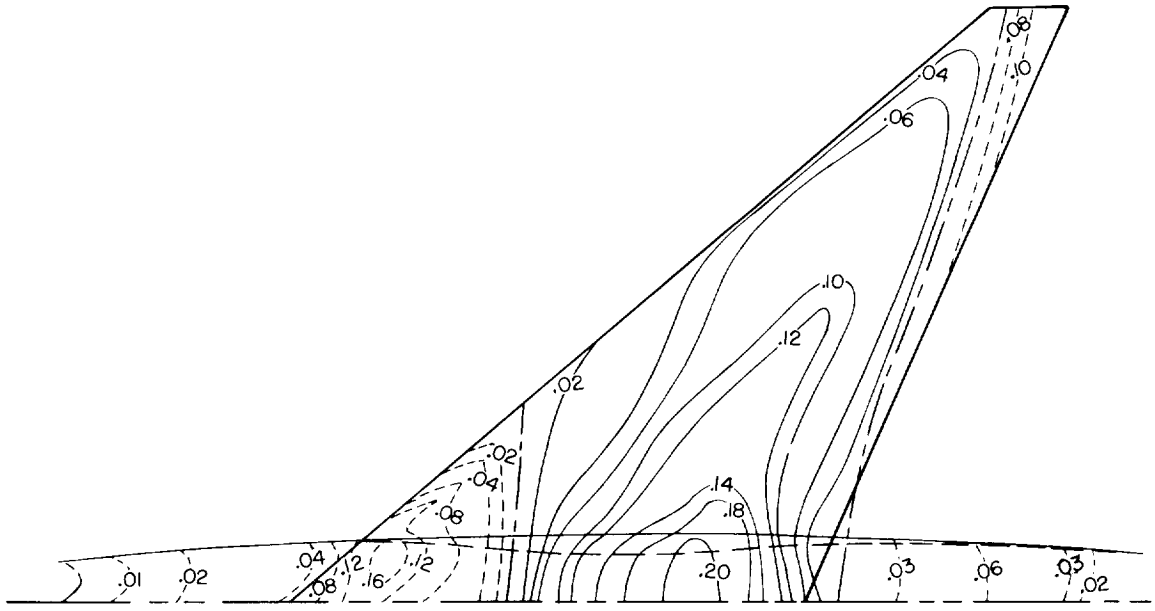

(b) M = 0.98.

Figure 9.- The pressure field induced over the wing and body due to a symmetrical M = 1.2 indentation. $\alpha = 0^{o}$. (Upper surface unless otherwise noted.)

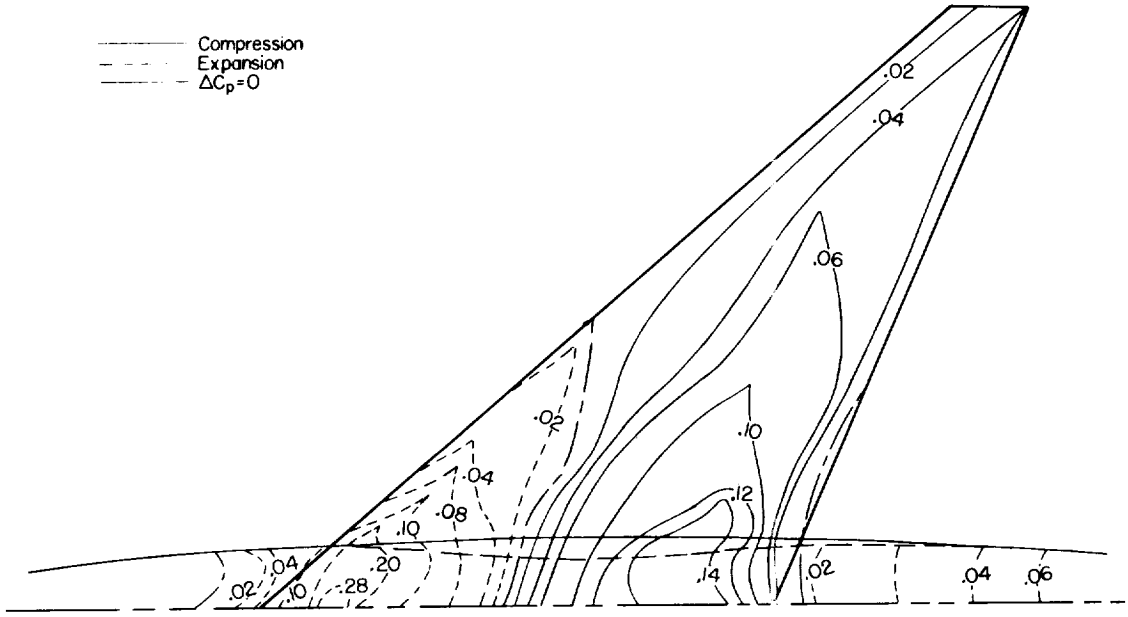

(c) M = 1.03.

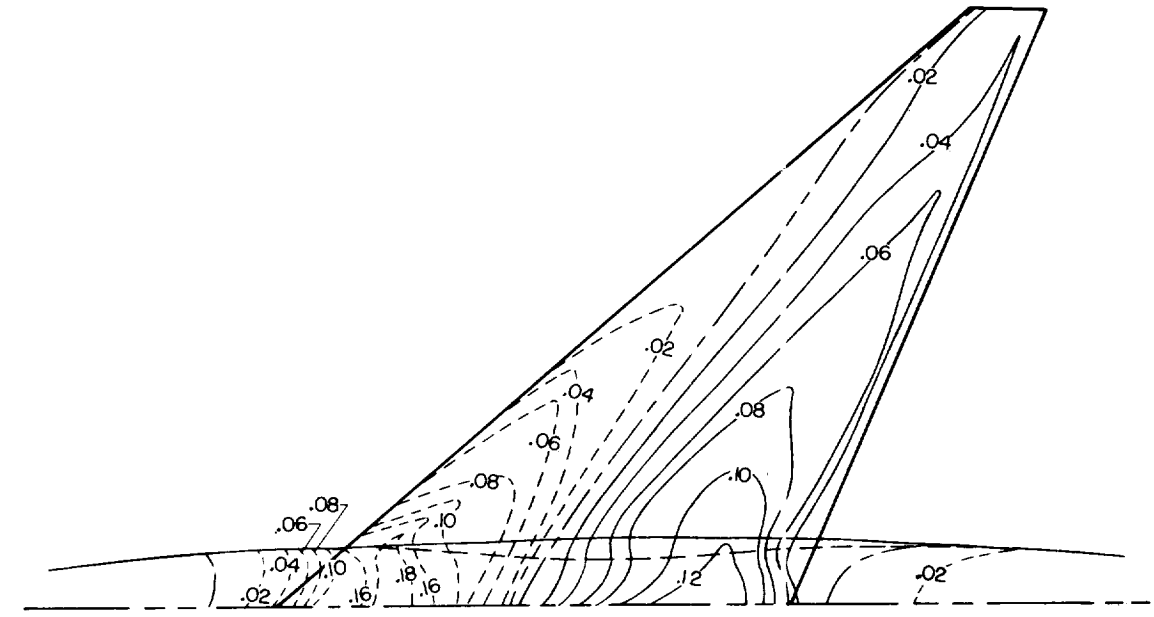

(d) M = 1.125.

Figure 9.- Continued.

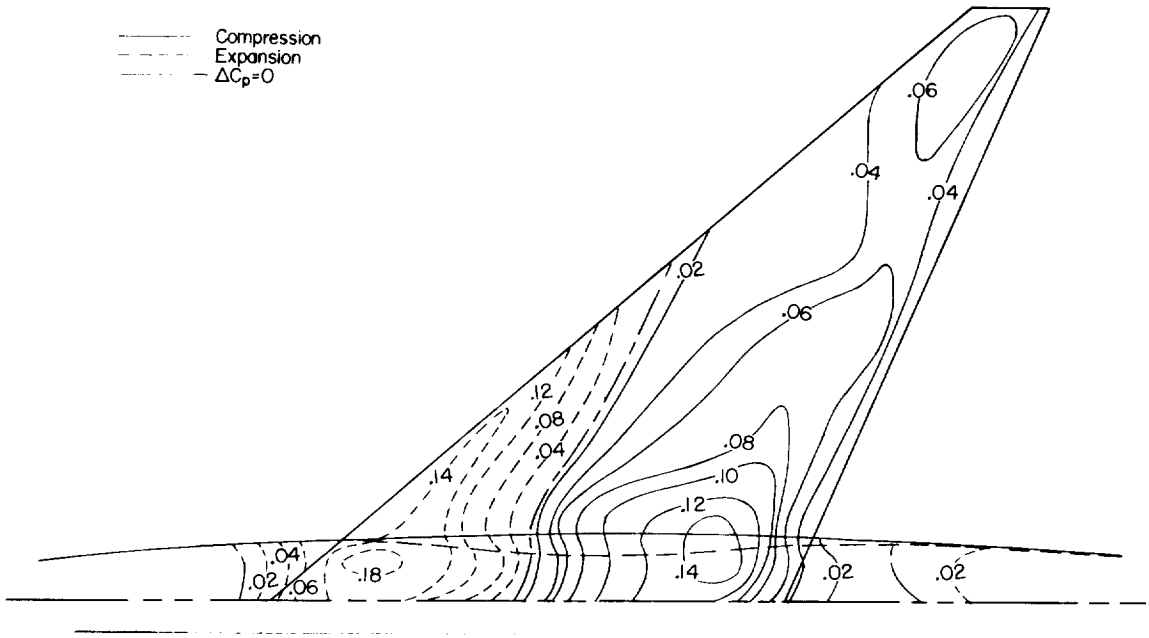

(e) M = 1.125; lower wing surface.

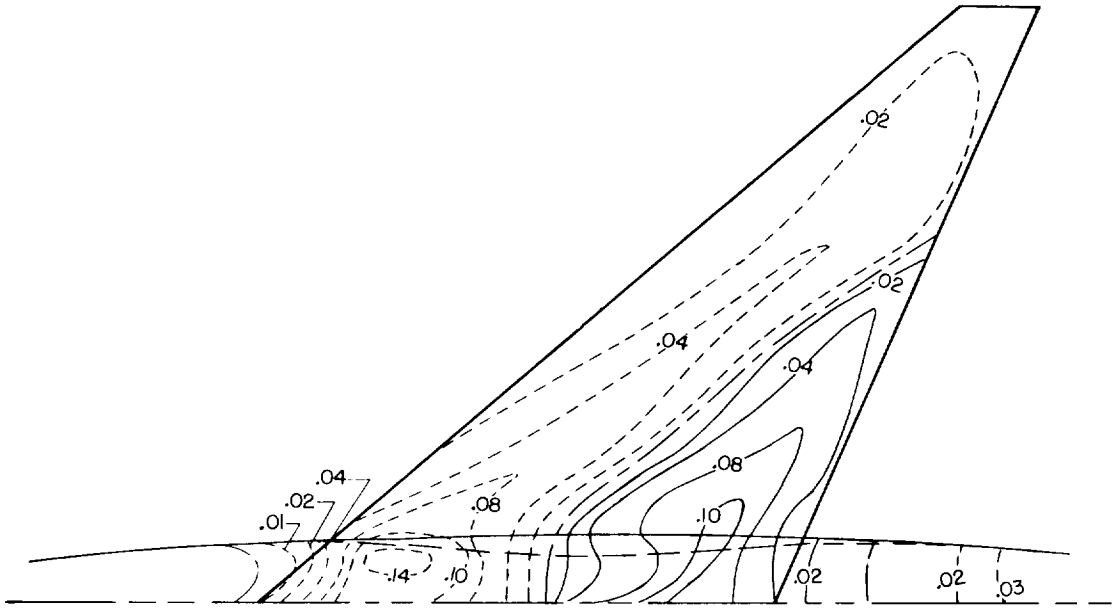

(f) M = 1.43.

Figure 9.- Concluded.

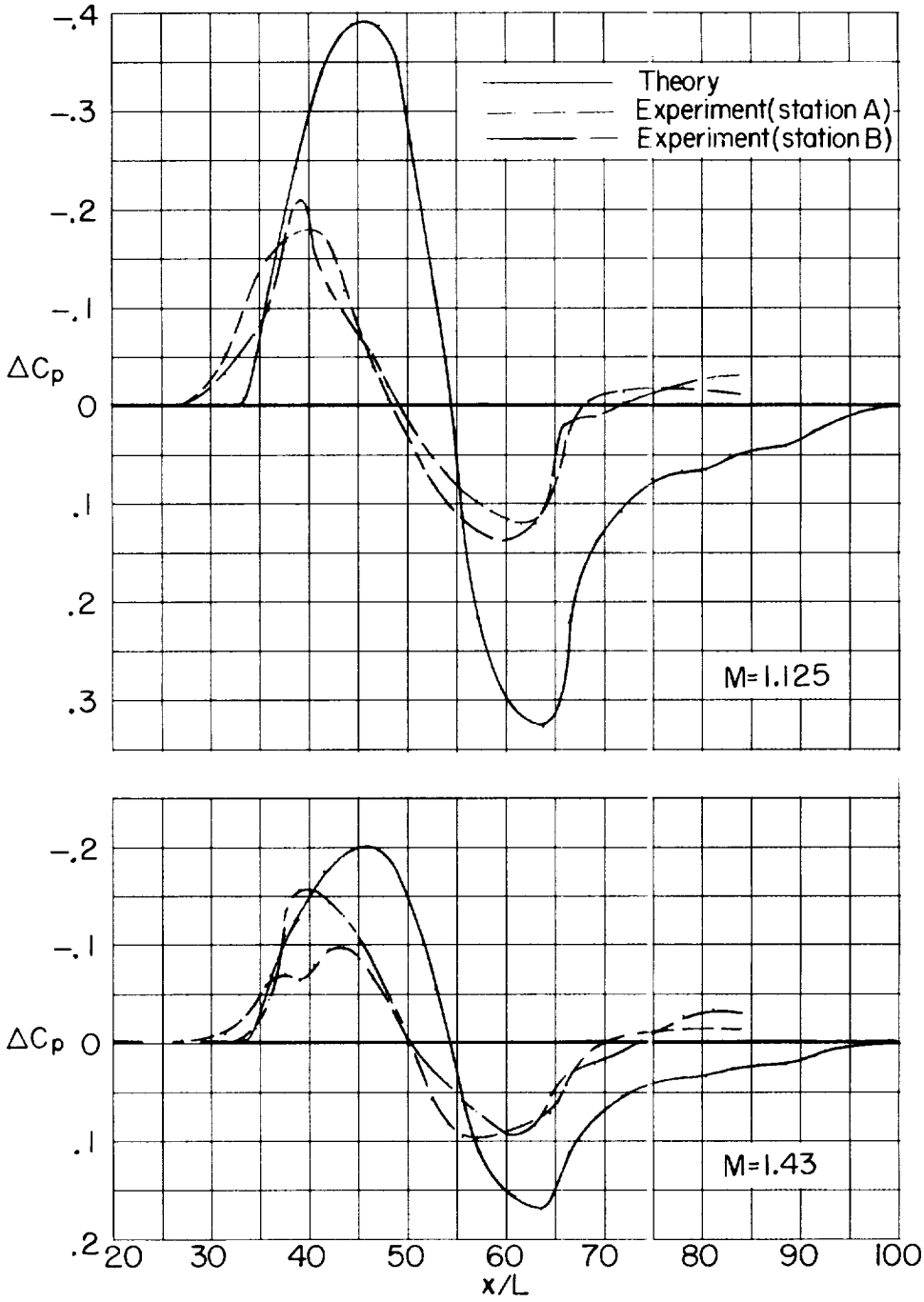

Figure 10.- Comparison of the theoretical and experimental pressure change over the upper surface of the body due to a symmetrical M = 1.2 indentation.

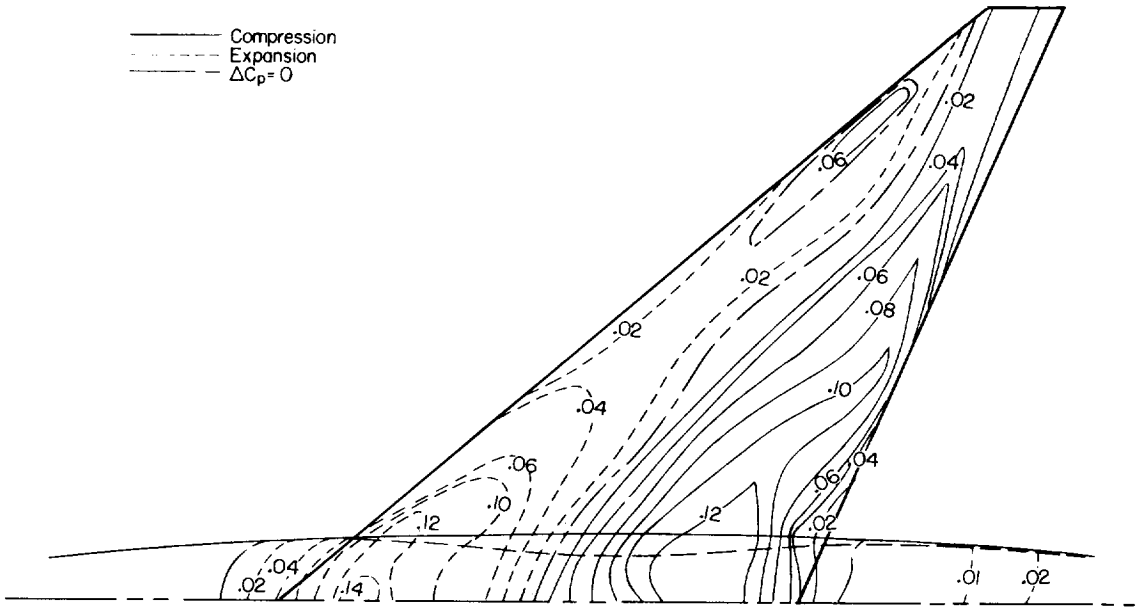

(a) M = 1.125; upper wing surface.

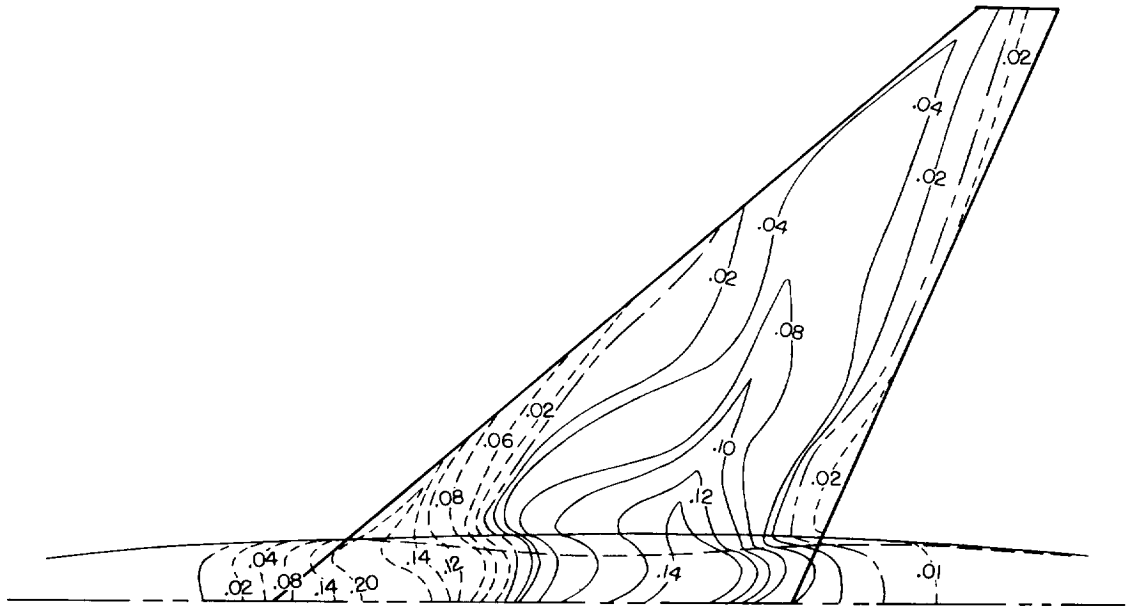

(b) M = 1.125; lower wing surface.

Figure 11.- The pressure field induced over the wing and body due to a symmetrical M = 1.2 indentation. $\alpha = 4^{\circ}$.

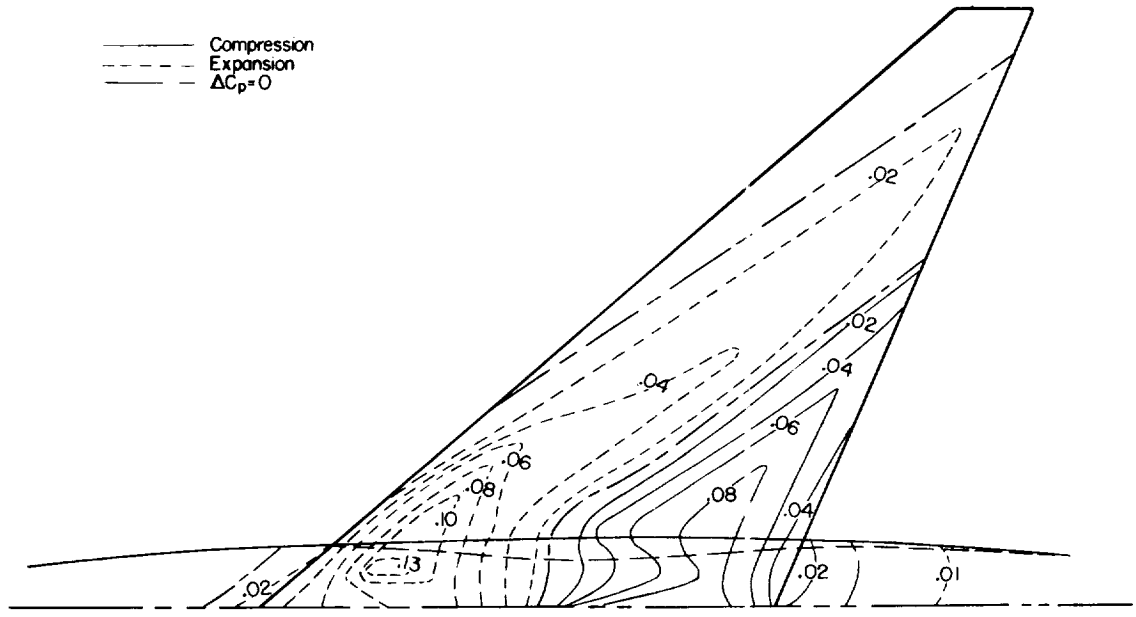

(c) M = 1.43; upper wing surface.

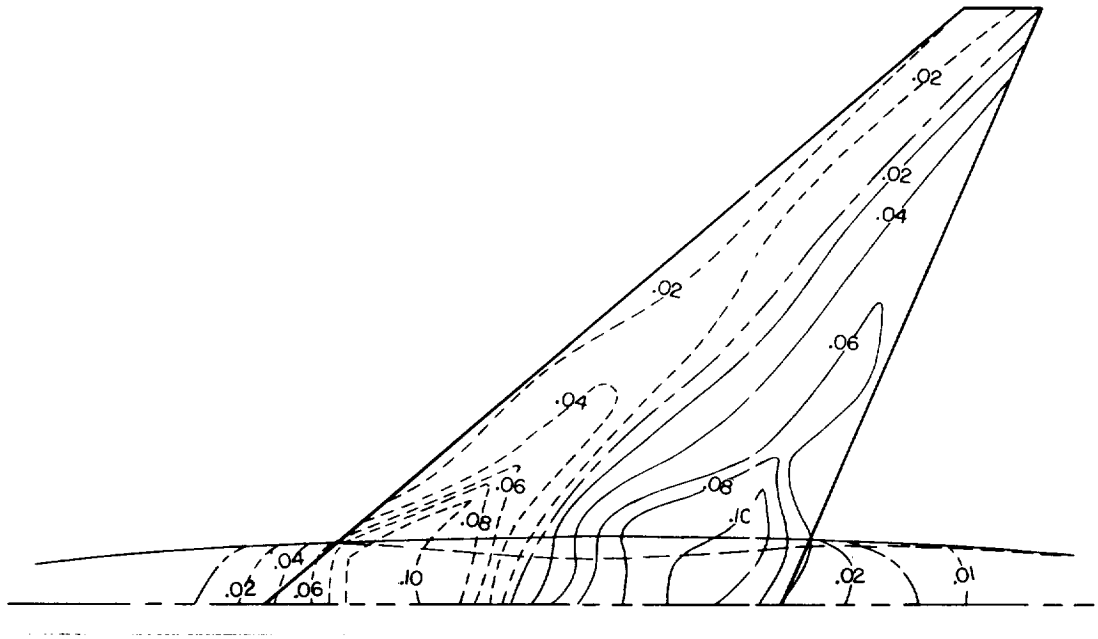

(d) M = 1.43; lower wing surface.

Figure 11.- Concluded.

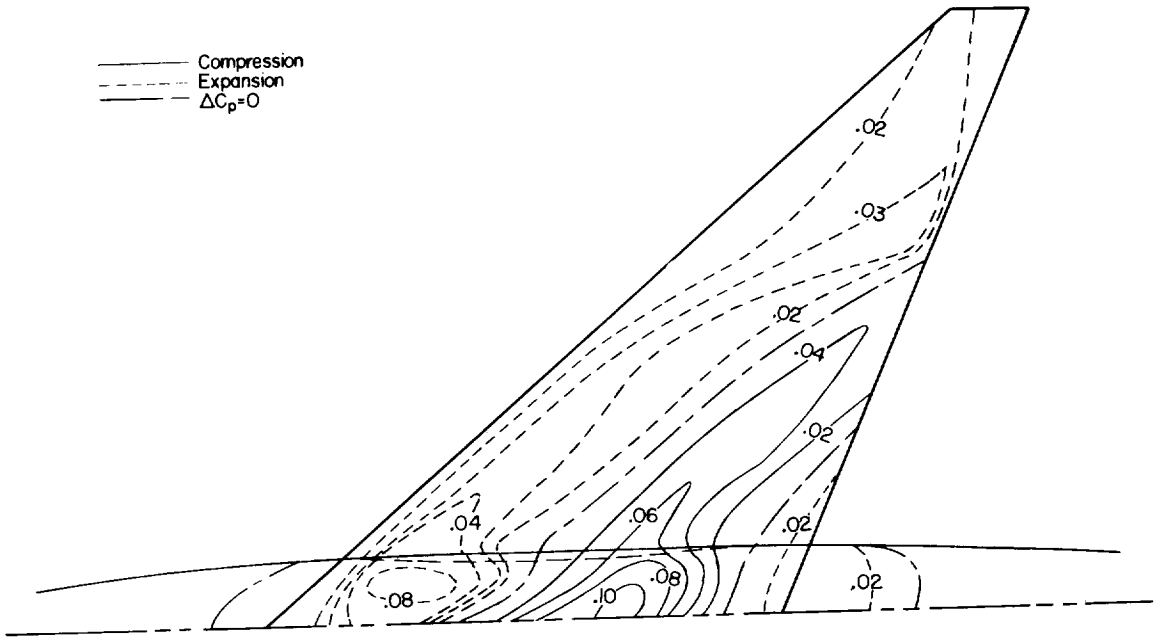

(a) M = 1.43; upper wing surface.

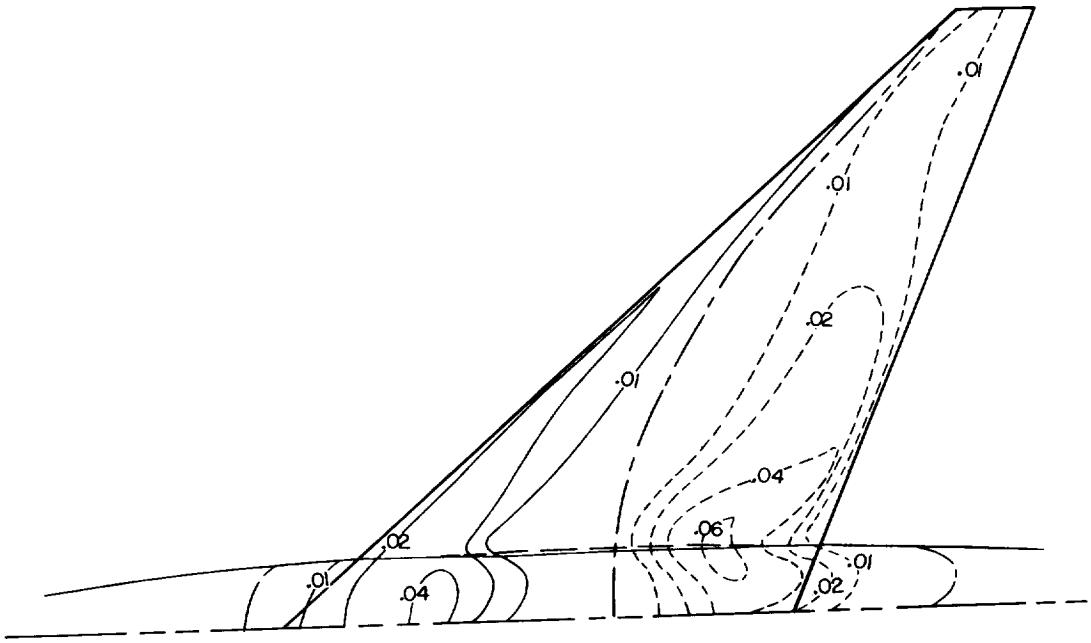

(b) M = 1.43; lower wing surface.

Figure 12.- The pressure field induced over the wing and body by a change from a symmetrical M = 1.4 indentation to an asymmetrical indentation. $\alpha = 4^{o}$.

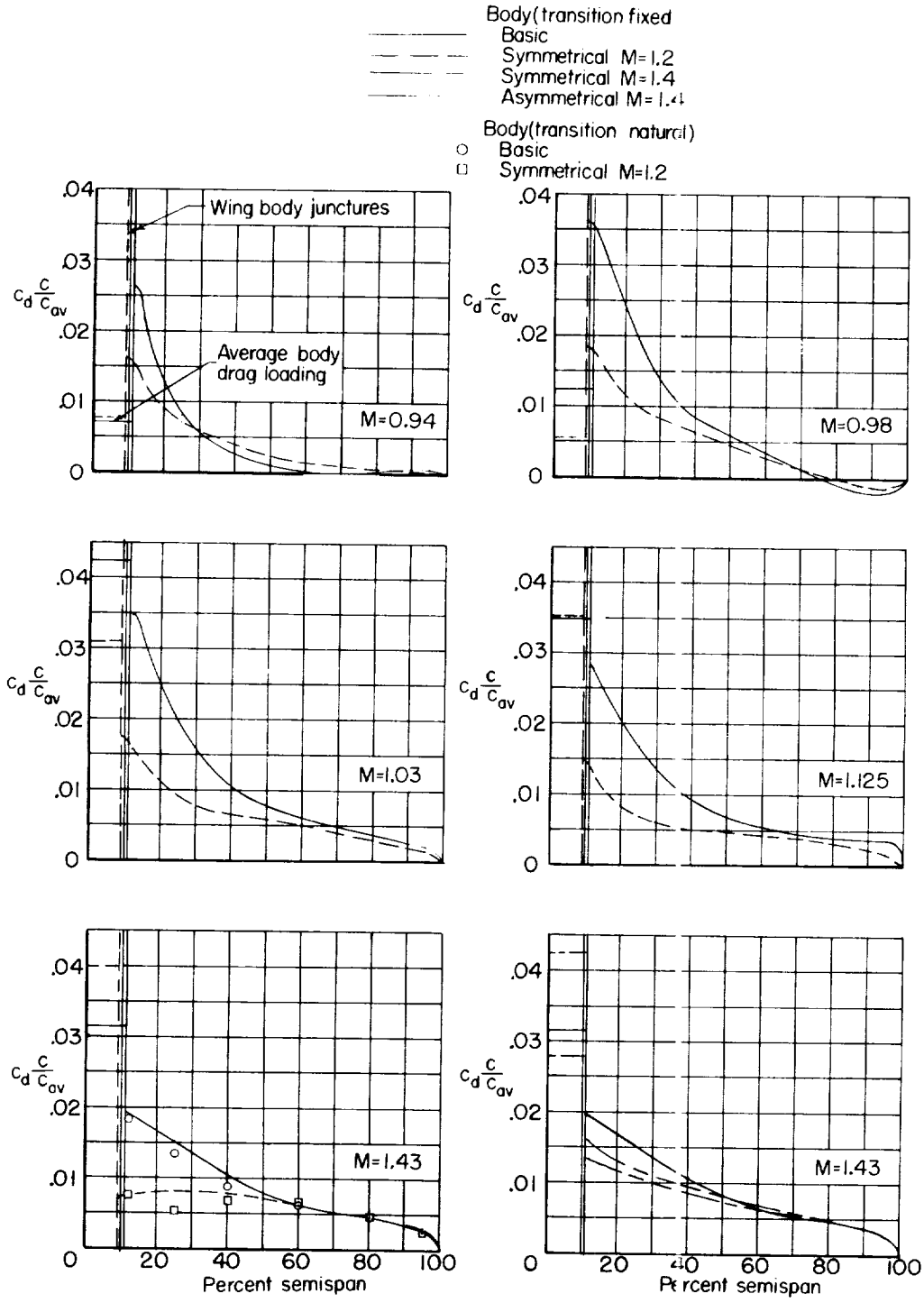

Figure 13.- The spanwise variation of drag loading coefficient for the wing in the presence of several bodies. $\alpha = 0^{\circ}$.

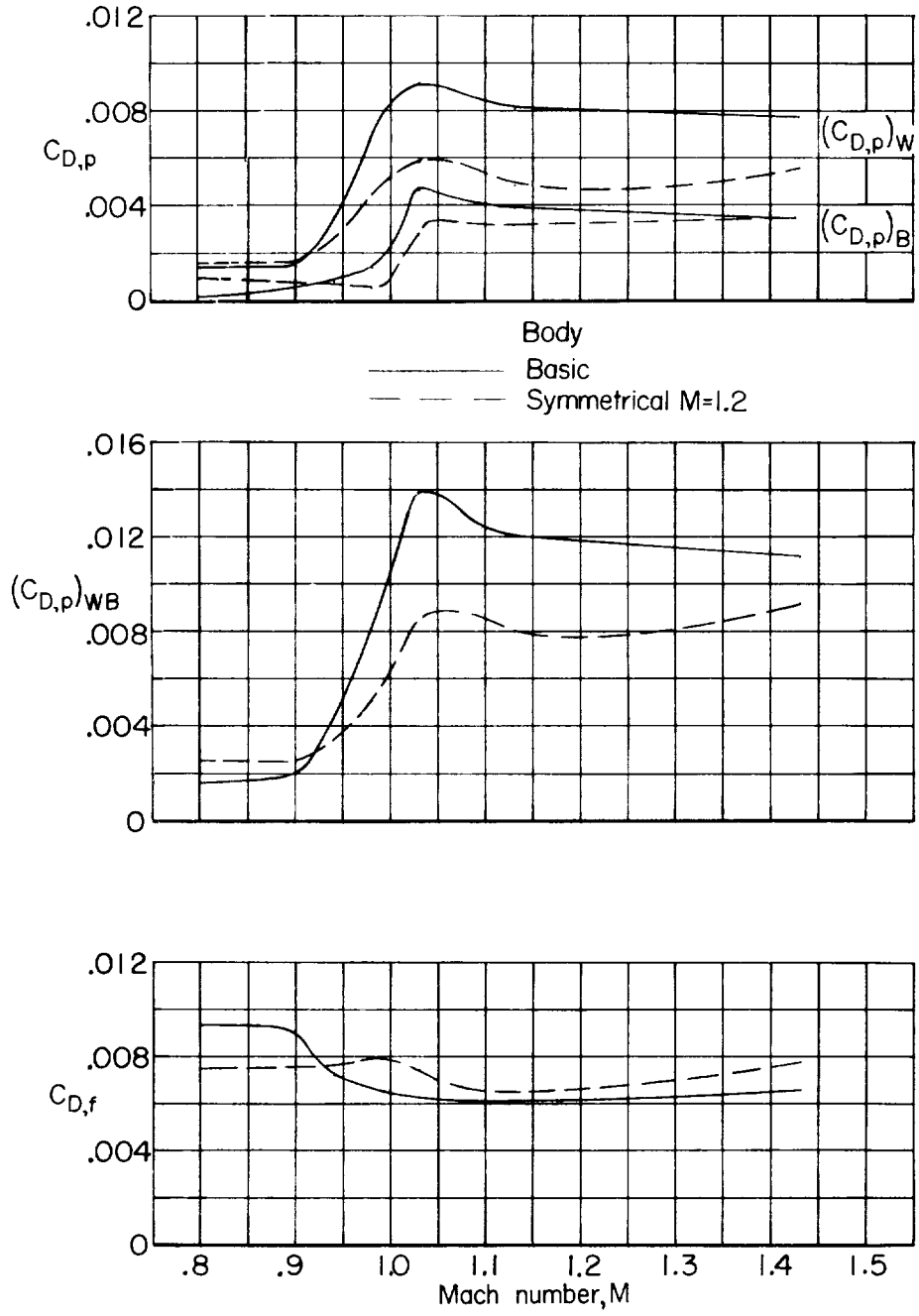

Figure 14.- The variation with Mach number of the wing pressure drag, the body pressure drag, the wing-body pressure drag, and the skin-friction drag for the basic and symmetrical M = 1.2 body and wing combinations. $\alpha = 0^{\circ}$.

56

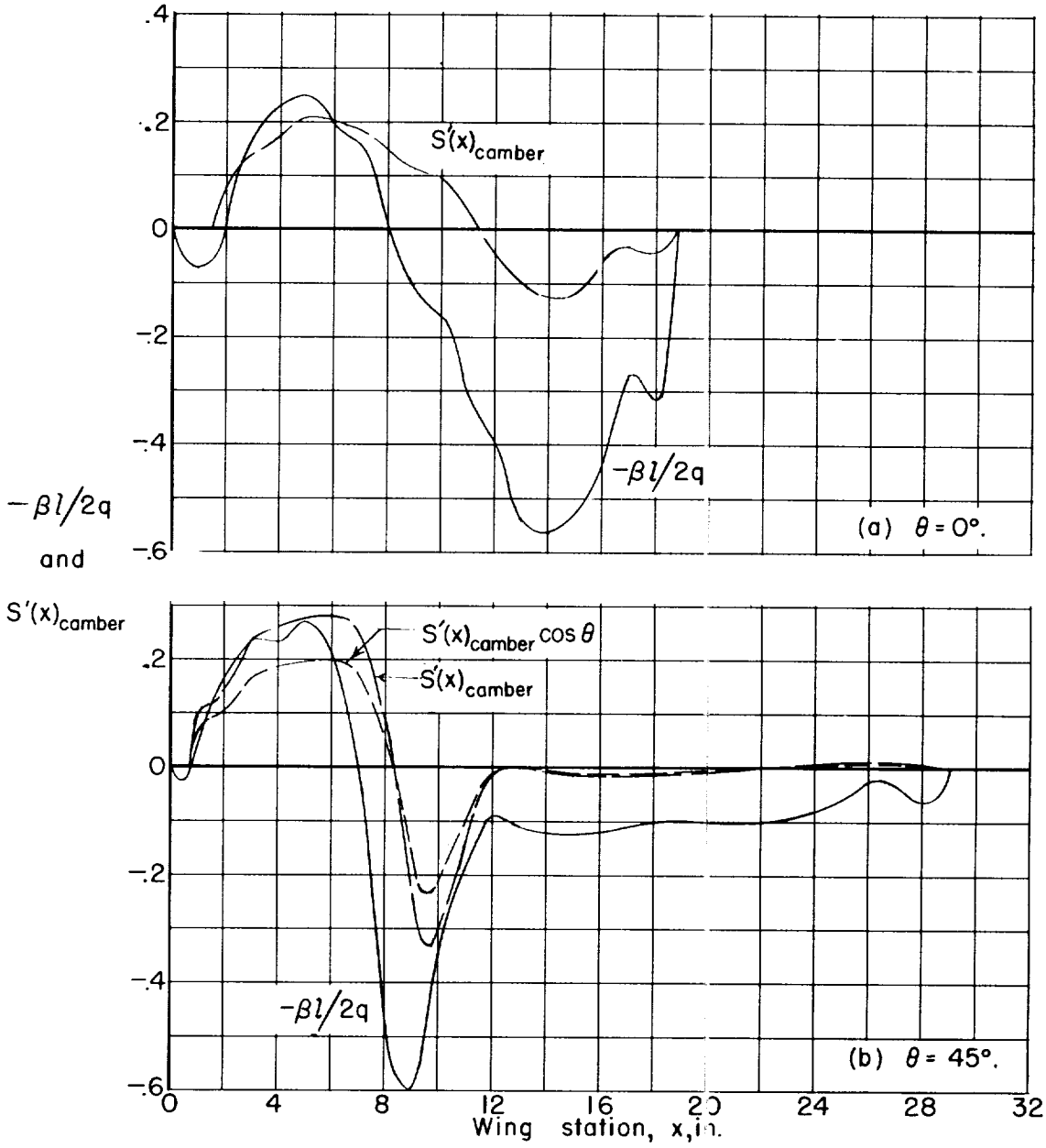

Figure 17.- Comparison of the distribution of $-\beta l/2q$ and the slope of the cross-sectional area distribution due to wing camber, including the effects of aeroelastic wing twist, for the wing—basic-body combination. $\alpha = 0°$; $M = 1.43$.

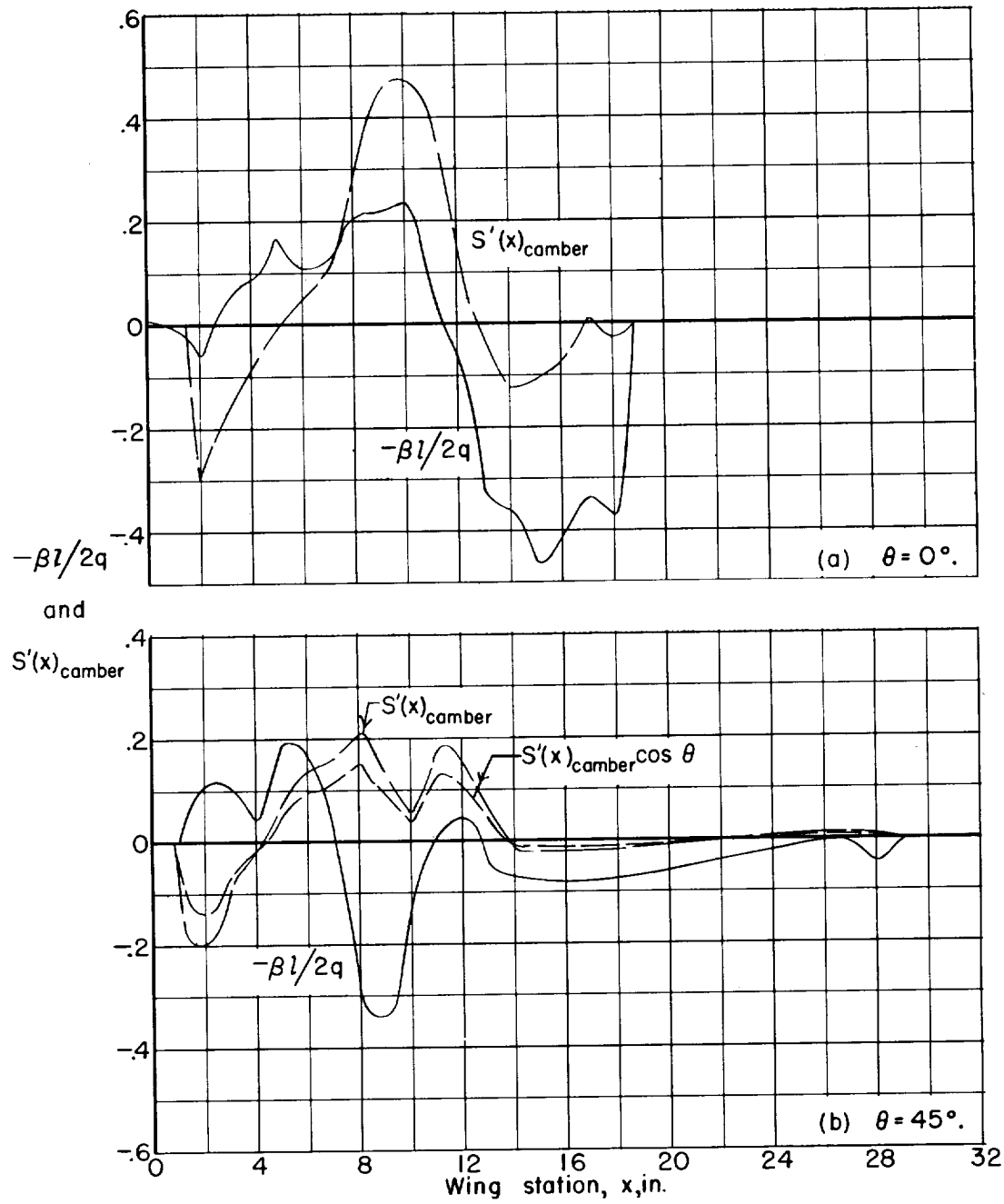

Figure 18.- Comparison of the distribution of $-\beta l/2q$ and the slope of the cross-sectional area distribution due to wing camber and body asymmetry, including the effects of aeroelastic wing twist, for the asymmetrical M = 1.4 body and wing combination. $\alpha = 0^{\circ}$; M = 1.43.

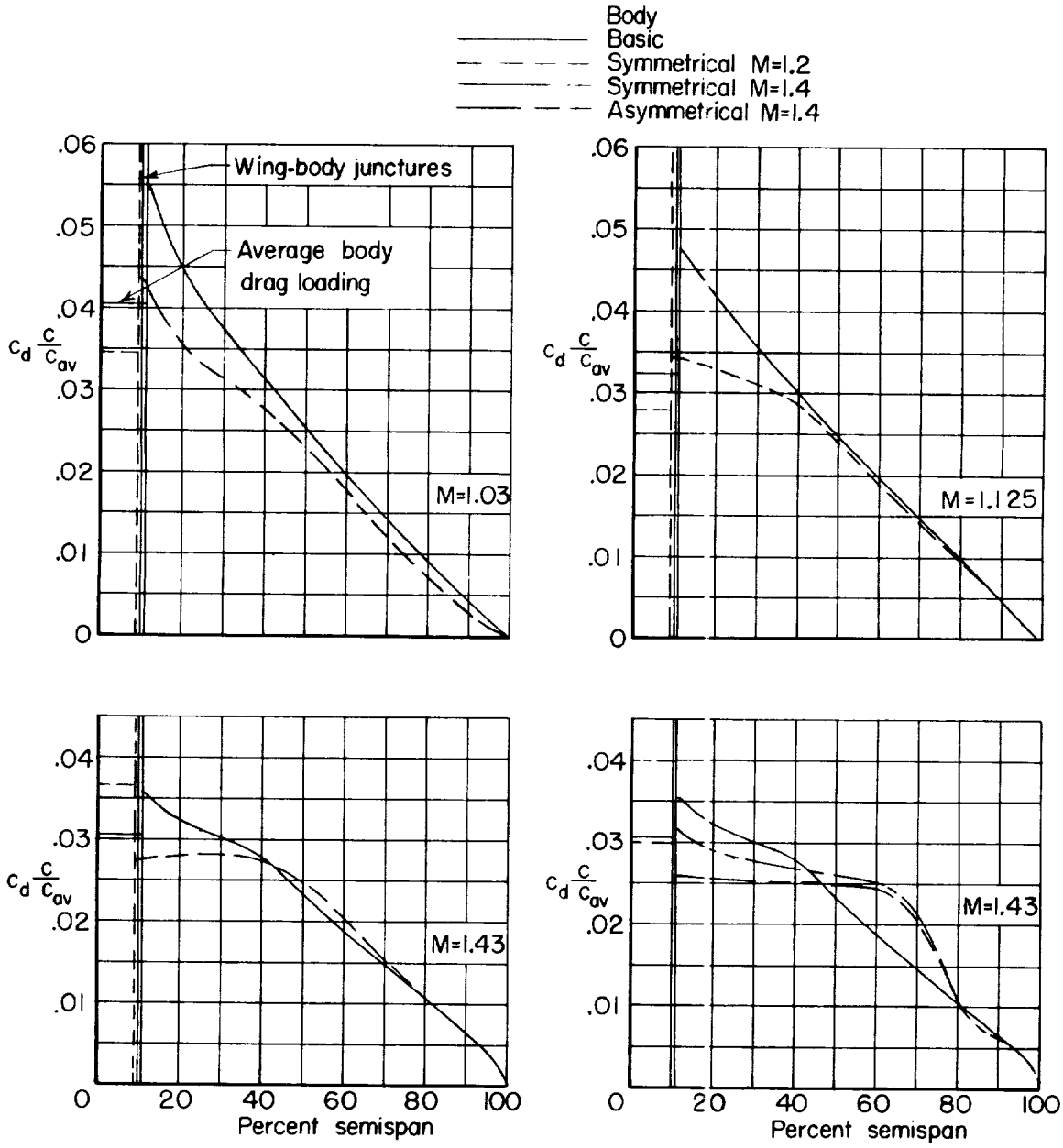

Figure 19.- Spanwise distribution of drag loading for the wing in the presence of several body shapes. $\alpha = 4^{\circ}$.

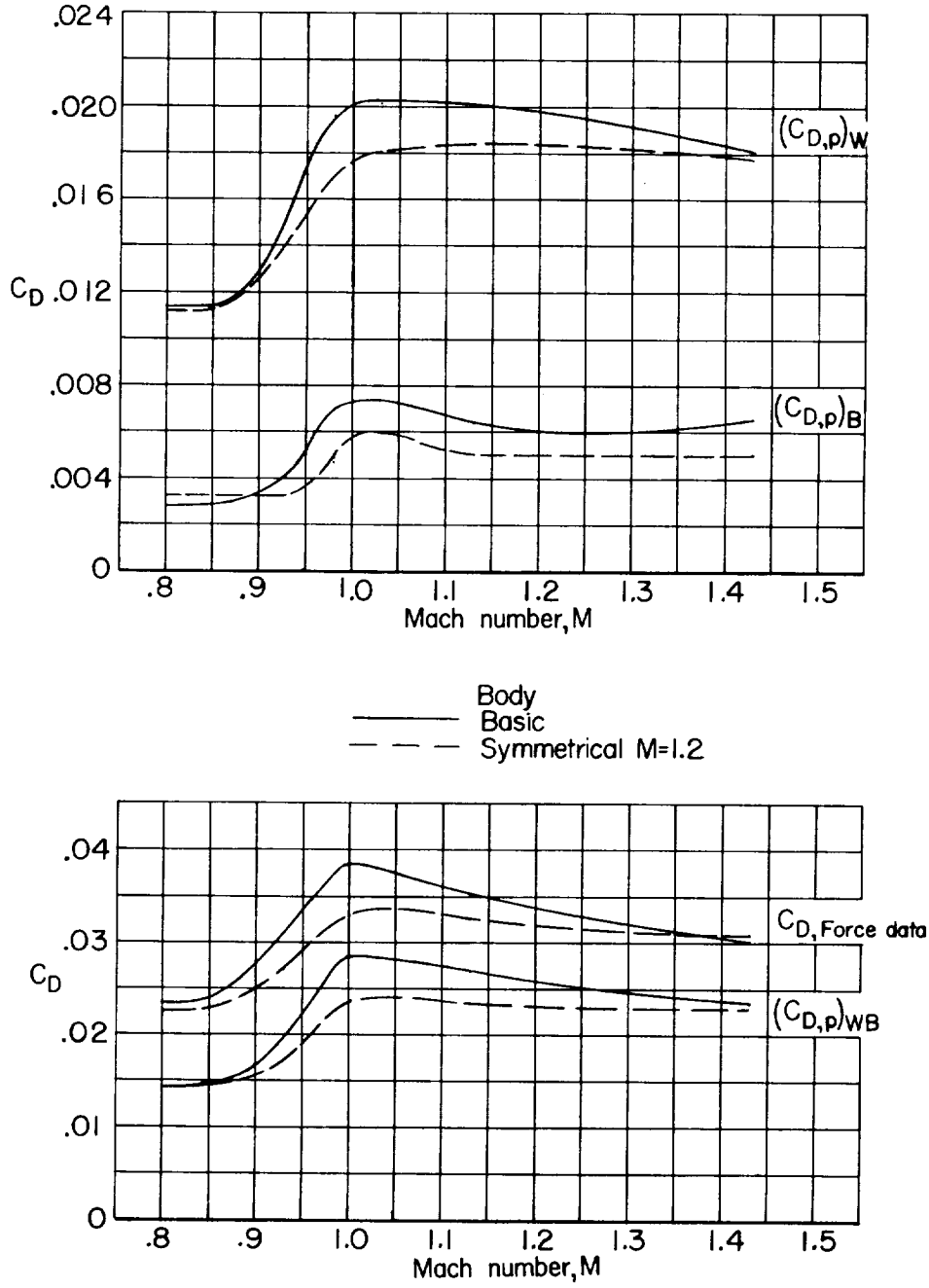

Figure 20.- The variation with Mach number of the wing pressure drag, the body pressure drag, the wing-body pressure drag, and the force test results of reference 6 for the basic and symmetrical M = 1.2 body and wing combinations. $\alpha = 4^{\circ}$.

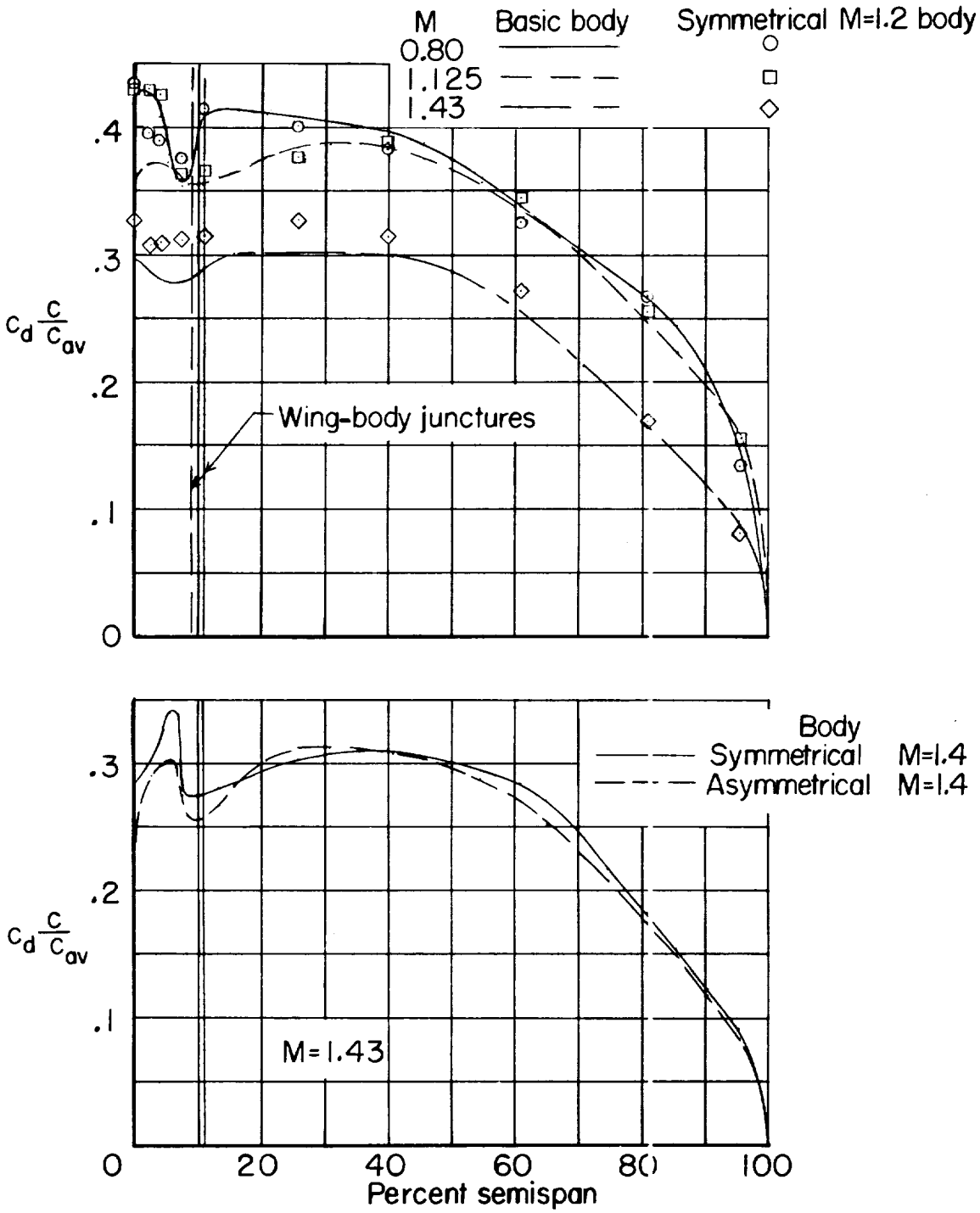

Figure 21.- Spanwise distribution of normal loading coefficient for several wing-body combinations. $\alpha = 4^{\circ}$.

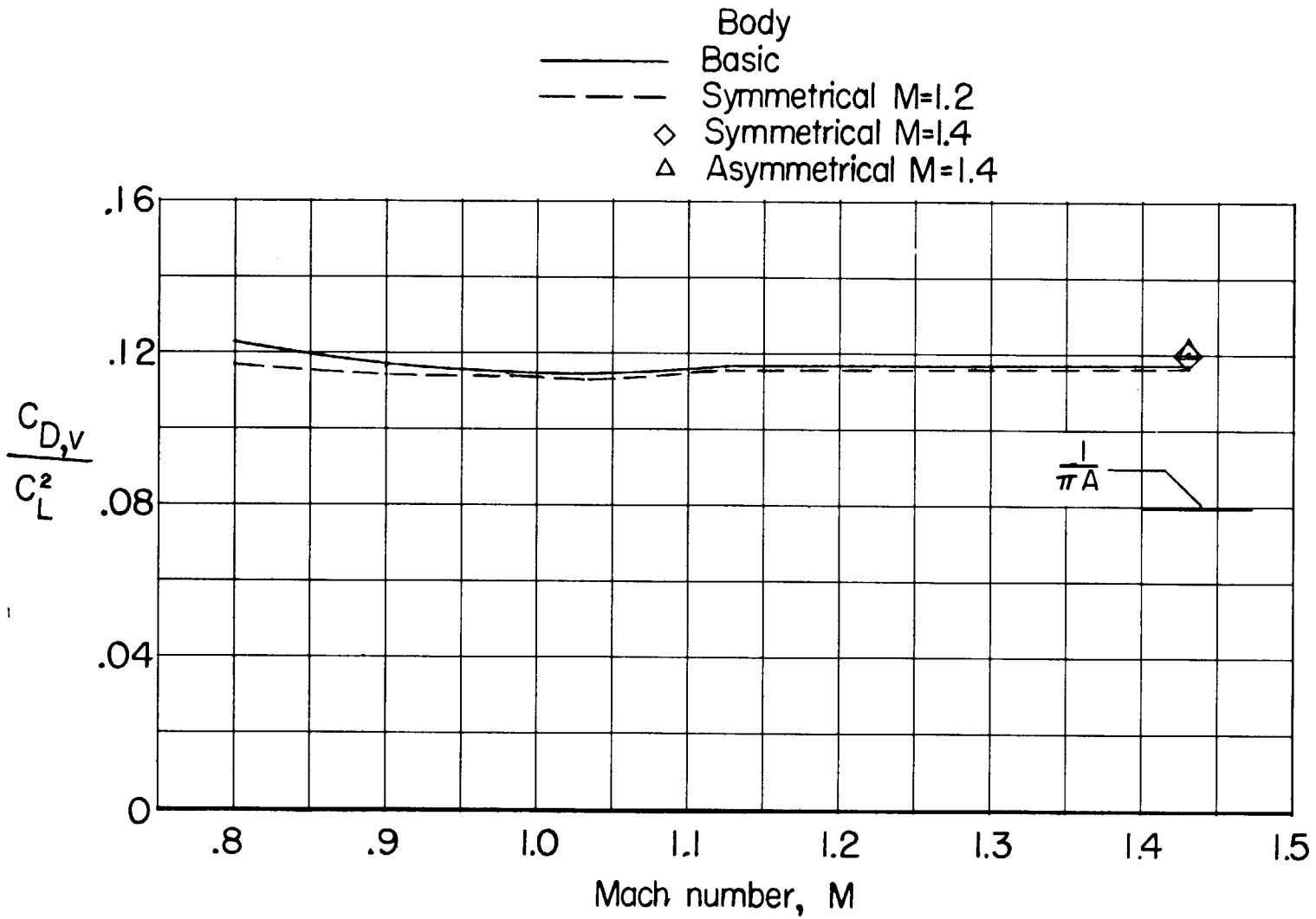

Figure 22.- Variation with Mach number of the vortex drag due to lift parameter for the basic and symmetrical M = 1.2 body and wing combinations. $\alpha = 4^{\circ}$.

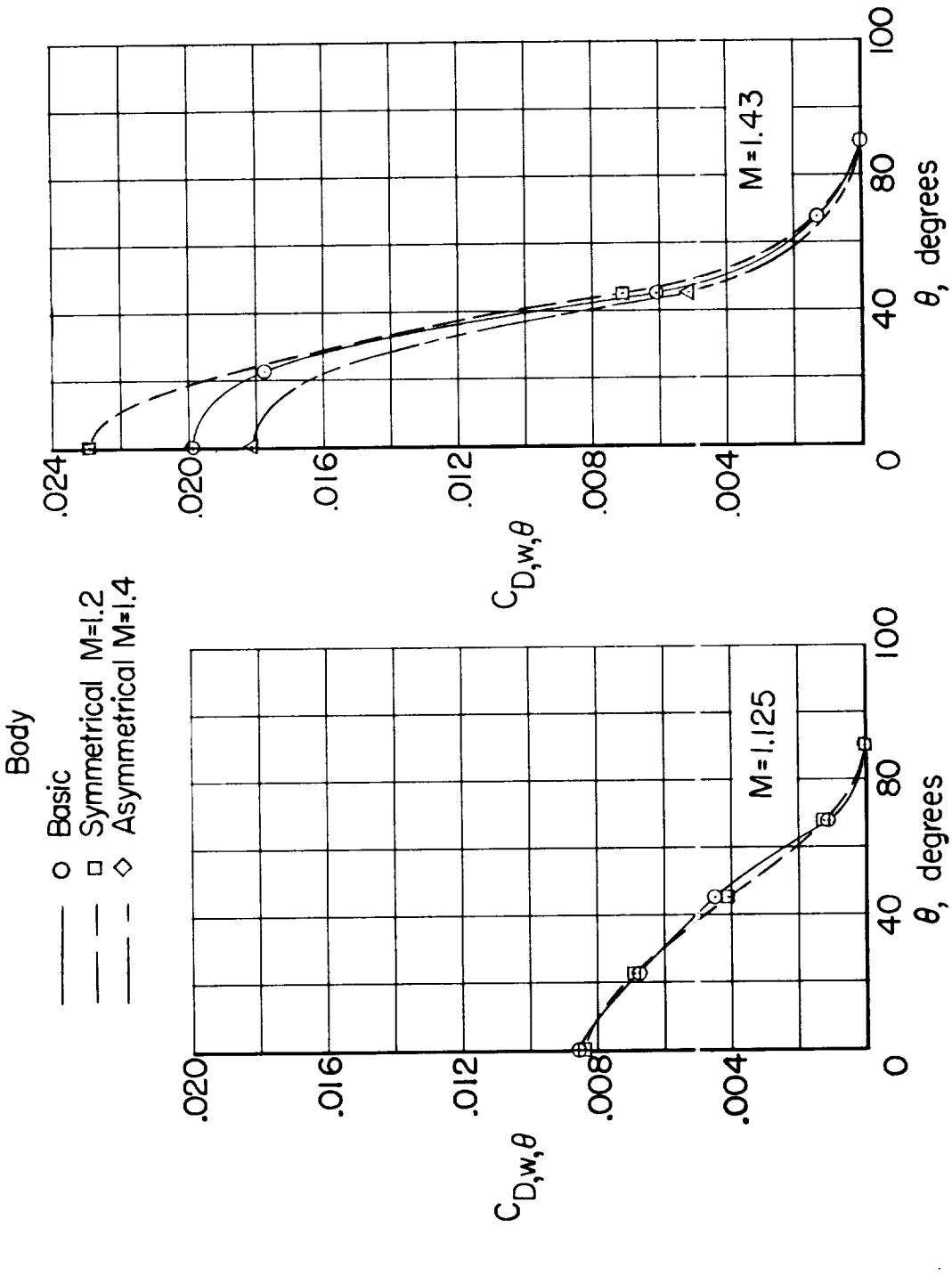

Figure 23.- Variation with the cutting-plane roll angle θ of the incremental wave drag due to lift for several wing-body combinations. $\alpha = 4^{\circ}$.

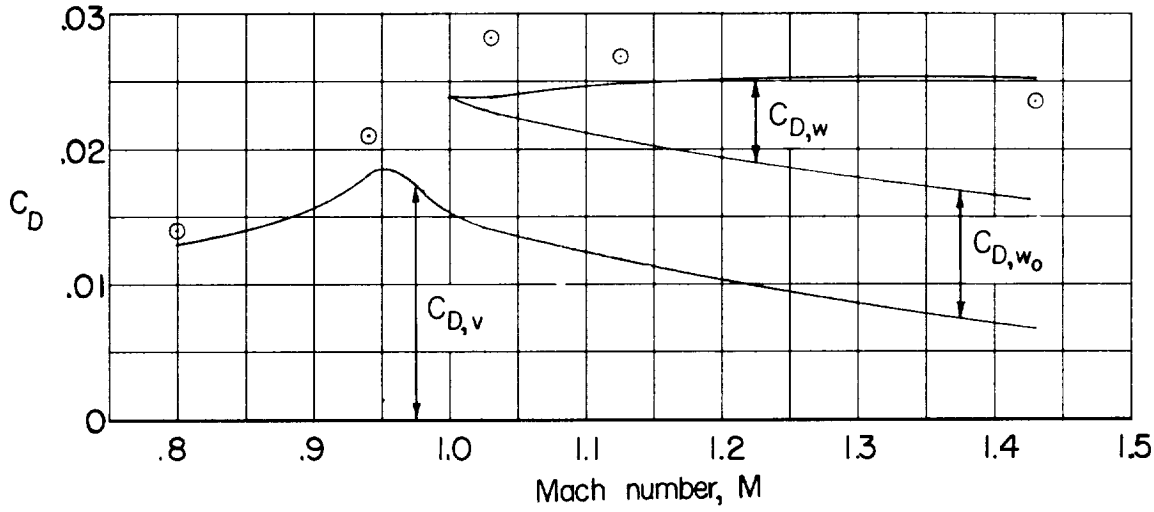

(a) Basic body.

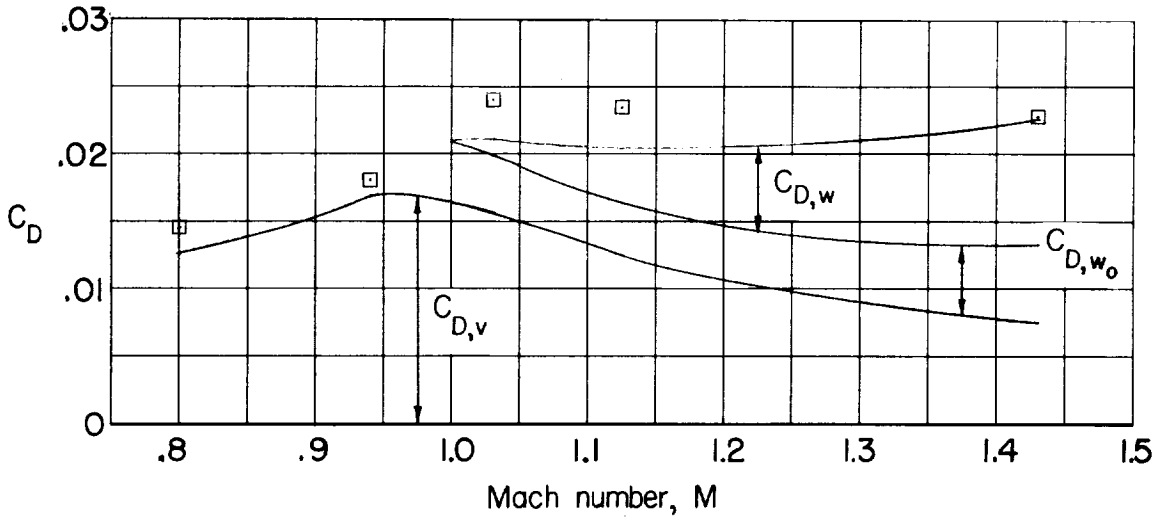

(b) Symmetrical M = 1.2 body.

Figure 24.- Comparison of the experimental and calculated drags for the basic and symmetrical M = 1.2 body and wing combinations. $\alpha = 4^{\circ}$. Symbols indicate experimental values.

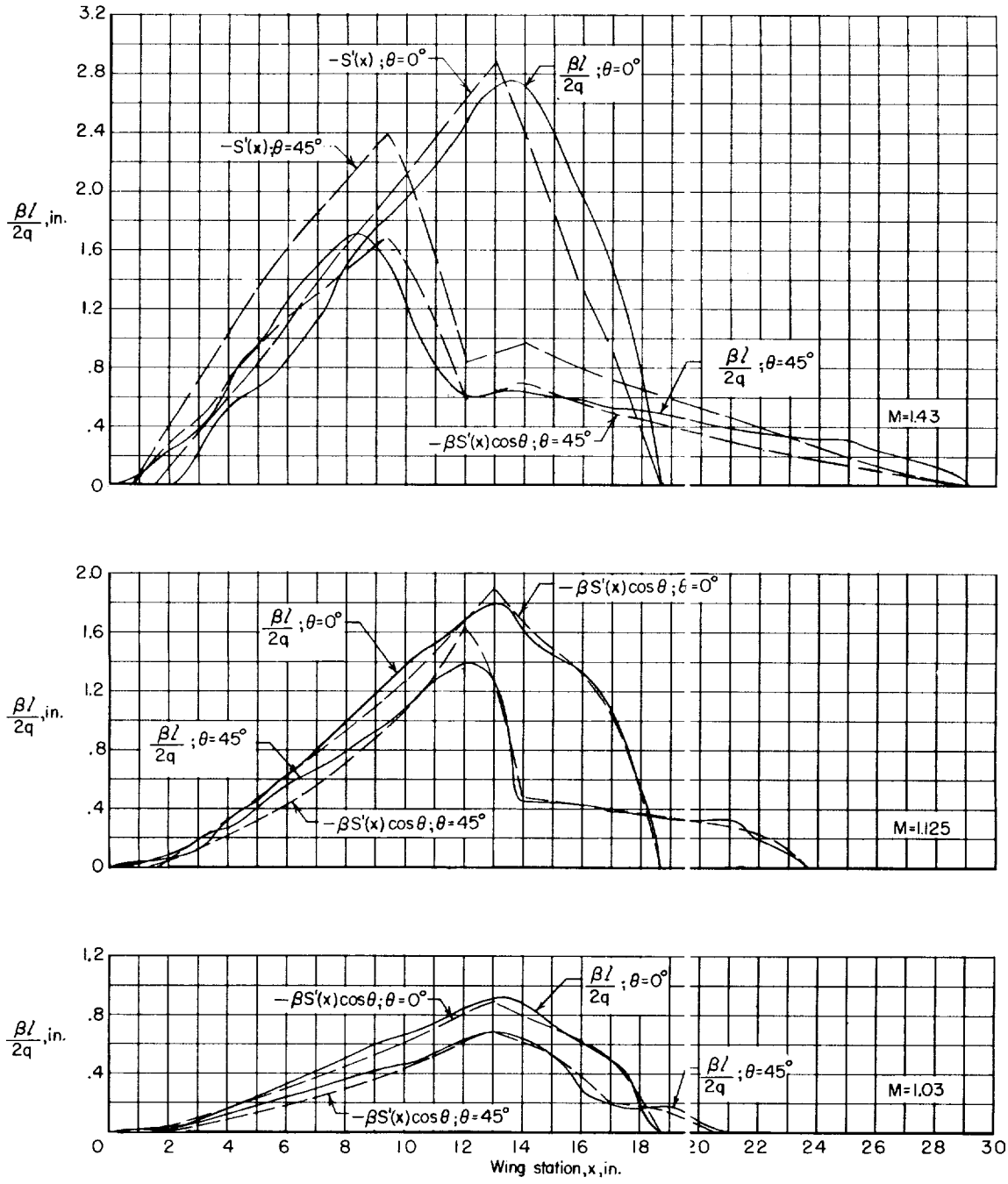

Figure 25.- Comparison of the distribution of $\beta l/2q$ and the slope of the area distribution due to angle of attack and wing camber for the wing—basic-body combination. $\alpha = 4^{o}$.

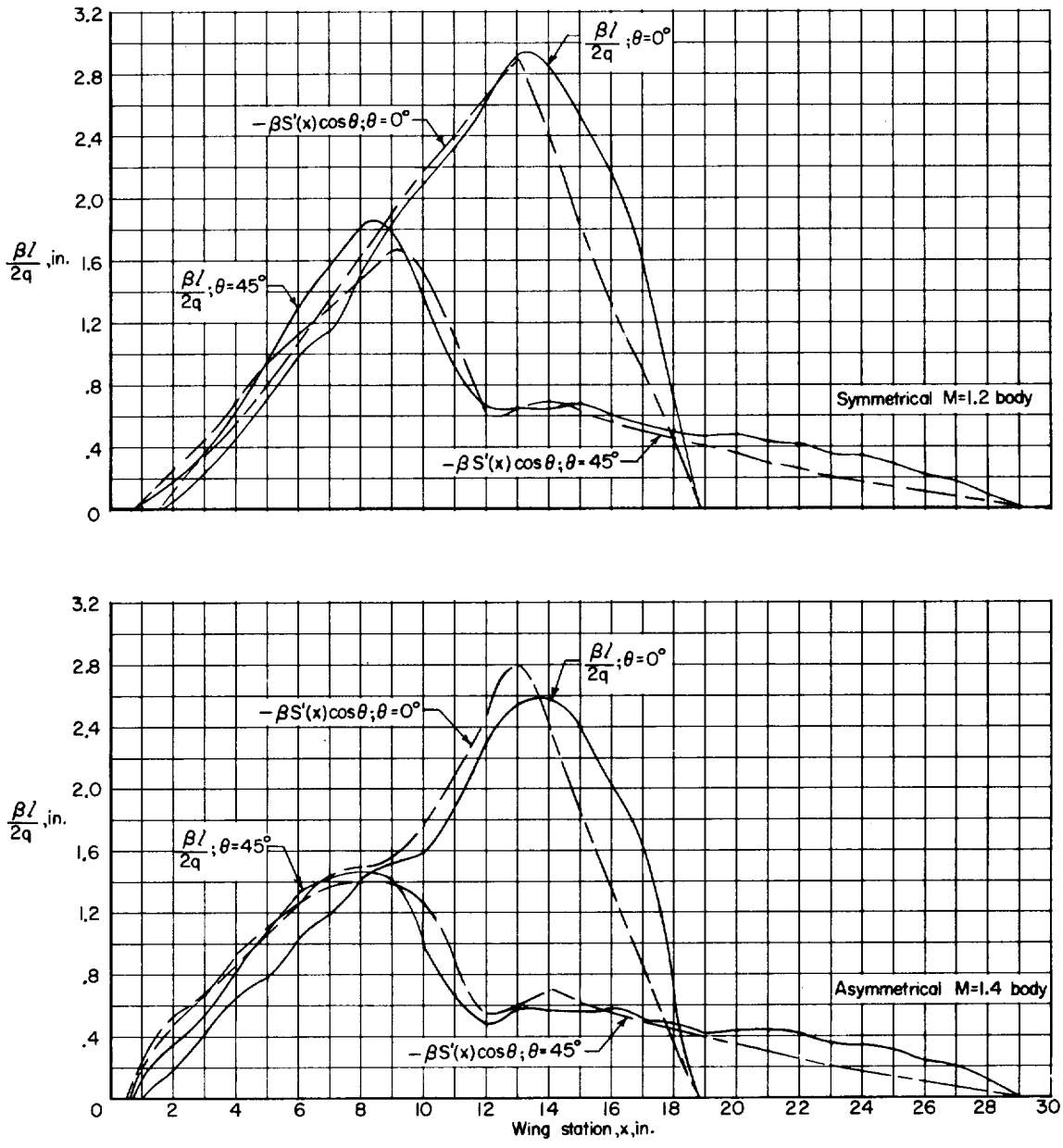

Figure 26.- Comparison of the distribution of $\beta l/2q$ and the slope of the area distribution due to angle of attack, wing camber, and body asymmetry for the symmetrical M = 1.2 and asymmetrical M = 1.4 body and wing combinations. $\alpha = 4^{\circ}$; M = 1.43.

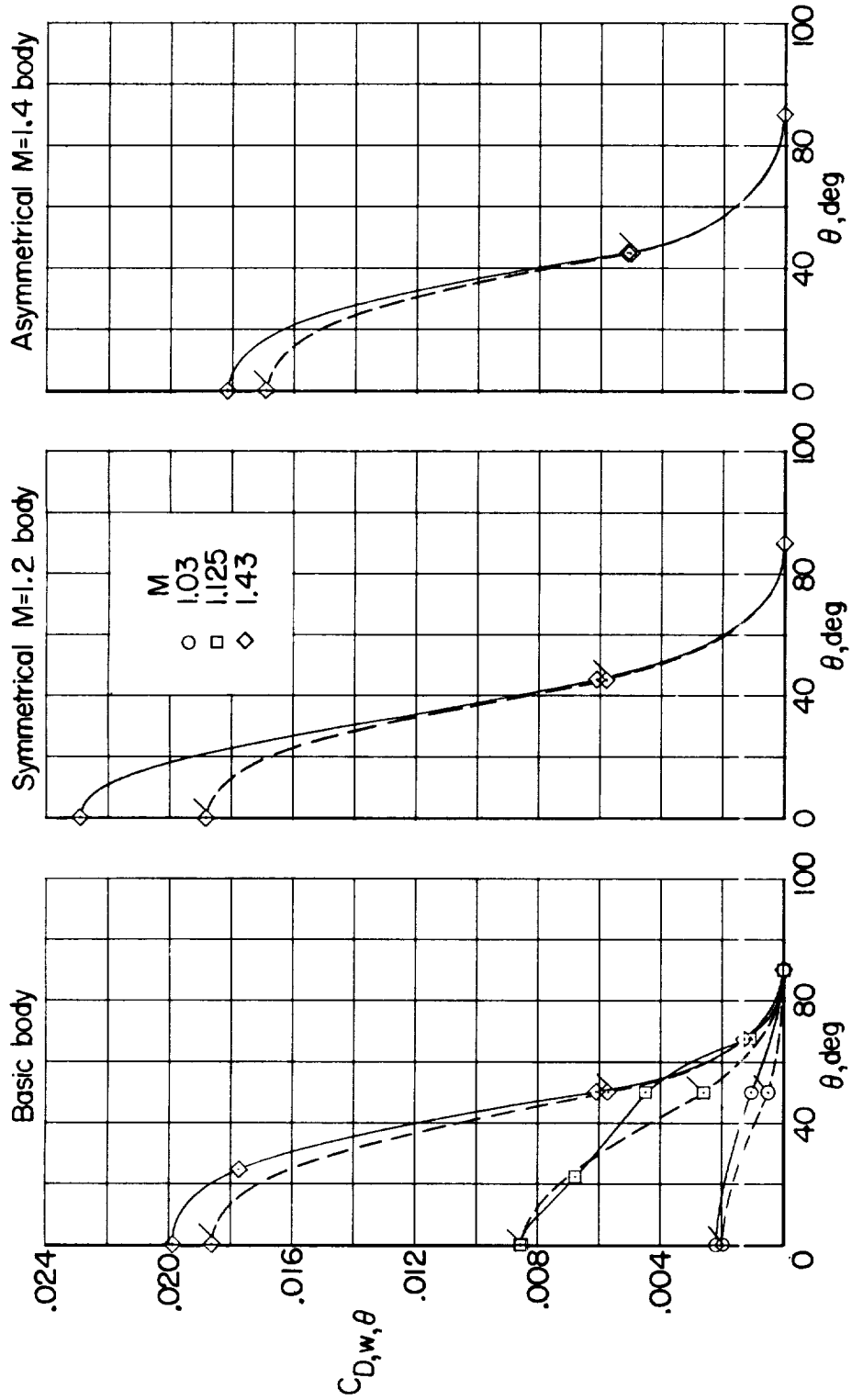

Figure 27.- Variation with cutting-plane roll angle θ of incremental wave drag due to lift for several wing-body combinations. Plain symbols indicate values calculated from distributions of $\beta l/2q$. Flagged symbols indicate values calculated from slope of cross-sectional area due to angle of attack, wing camber, and body asymmetry. $\alpha = 4^{\circ}$.